DIPLOMA THESIS

Porous Medium Flow Simulation

in a Brush Seal with Radial Clearance

Written at

Institute for Energy Systems and Thermodynamics

Faculty of Mechanical and Industrial Engineering

Vienna University of Technology

Under direction of

Ao.Univ.Prof. Dipl.-Ing. Dr.techn. Reinhard Willinger

By

Mehmet Germen

0826803

Gentzgasse 14/14/5

1180 Vienna

Vienna, November 2012

ABSTRACT

The application of sealing technologies in the field of turbo machinery brings a significant improvement at the turbo machine efficiency.

The sealing technologies undergo constant development and improvement. If it is thought that the first brush seal application was tried in 40s, it can be rather said that the progress and development is unstoppable.

One of the most important sealing technologies is brush seal technology. This sealing technology has an important role to improve the internal flow system in turbo machinery. Big power requirements from the aero engine gas turbines driven to higher pressure ratios, by-pass ratios and turbine inlet temperatures. Due to these effects, the air flows in the internal air system and thermodynamically loses increase. Internal flow system is important for the engine efficiency. Therefore the aim is always reducing the internal airflows therewithal increasing thermodynamic efficiency. Brush seals give this opportunity for turbo machines. On the other hand, labyrinth seal technology is also very well developed but the leakages are still high. Brush seals fulfill such conditions. But brush seals have also different disadvantages like bristle wearing und etc. Therefore designers are always looking for new designs. And one of them is brush seal with radial clearance. With these designs, it is tried to reach optimum clearance between rotor and bristle tips. It is tried to avoid from the leakage like labyrinth seals, at the same time avoid from the wearing problem like in brush seals.

This work’s intention is to develop and to simulate a model which has optimum clearance with brush sealing and comparing with existing investigations.

ACKNOWLEDGMENTS

I would like to thank Ao.Univ.Prof. Dipl.-Ing. Dr.techn. Reinhard Willinger for giving me an opportunity to work on the thesis and for supporting me during that time.

TABLE OF CONTENTS

FIGURE INDEX

TABLE INDEX

NOTATION

A	$[m^2]$	Total inlet height area $A = (R^2 - r^2)\pi$
g	$[m/s^2]$	Acceleration of gravity
$\check{c}$	[-]	Inertia coefficient
F_{fact}	$[\sqrt{K}\ s]$	Flow factor
H	[m]	Total height
h	[m]	Elevation/Piezometric height
h_{bf}	[m]	Bristle free height
h_{fh}	[m]	Fence height
h_1	[m]	Inlet height
k	[m/s]	Conductivity coefficient
$\dot{m}$	$[kg/s]$	Mass flow rate
p	[Pa]	Static pressure
$\bar{p}$	[Pa]	Mean pressure
p_a	[Pa]	Absolut pressure
p_d	[Pa]	Downstream pressure
p_{nd}	[-]	Dimensionless pressure
p_u	[Pa]	Upstream pressure
R_p	[-]	Pressure ratio
T_{avg}	[K]	Average temperature
v	$[m/s]$	Flow velocity
v_s	$[m/s]$	Surface velocity
x	[m]	Distance in x direction
y	[m]	Distance in y direction

Y	[-]	Normalised radial distance coordinate
γ	$[N/m^3]$	Specific weight
ε	[-]	Porosity coefficient
K	$[m^2]$	Permeability
μ	$[kg/m\ s]$	Dynamic viscosity
υ	$[m^2/s]$	Kinematic viscosity
ϱ	$[kg/m^3]$	Density
ϕ	[^{o}]	Lay angle
ψ	[-]	Stream function

ABBREVIATION

CFD	Computational Fluid Dynamics
SFC	Specific Fuel Consumption
EGT	Exhaust Gas Temperature
HPT	High Pressure Turbine
ACC	Active Clearance Control
MTBF	Mean Time Between Failures
GE	General Electric
FEM	Finite Element Method
MTU	Motoren- und Turbinen-Union GmbH
HP	High Pressure
LP	Low Pressure
BC	Boundary Condition

1. Introduction

Internal flow system in turbo machinery is important for the engine efficiency. The optimum flow structure is always desired. Therefore the aim is always reducing the internal airflows while increasing thermodynamic efficiency. Some sealing applications are used to reach this goal. One of the most common sealing applications is labyrinth seals. Labyrinth seals are very well developed but the leakages are still high. Therefore as alternative to the labyrinth seals, brush seal is improved. The leakage flow decreases dramatically. But this time, some other problems appear with brush sealing. With brush sealing, it is tried to close the gap between rotor and stator, so brush is used for it. But the bristle tips in brush touch to the rotor and it caused to the wearing. Also with pressure gradient in brush, it caused blow-down effect too. Finally brush seal with clearance is tried to reach optimum gap between rotor and bristles tips. Thus it is desired that the bristle tips don't touch on rotor surface but the clearance is not wide like in labyrinth seals. Bayley and Long and Chew et al. have done some experiments and simulations. They published them. These researches are used in present work as a reference.

In this work, the simulations are firstly applied to reach experimental data from Bayley and Long [1] with compressible and incompressible flow simulations. After capturing data, the model is improved and it is designed with radial clearance. With these simulations, it is tried to reach the data from Chew et al [11] who calibrates the experimental data from Bayley and Long. At the end of this work, results are given and the effect of radial clearance on the results is showed.

2. Sealing Technologies

2.1 Sealing in Gas and Steam Turbines

In this section firstly given the general information about the sealing in gas and steam turbines like the characteristic of turbomachine which has an important role to understand why we need sealing, sealing benefits, types and locations and material and environmental conditions.

2.1.1 Turbomachine Characteristic

To understand the most commonly used sealing technologies, we should firstly look at into the turbomachines characteristic. Turbomachines are not simple constructions. Some of them are with small dimensions and some of them are huge constructions where you can almost walk through. Examples for different constructions can be seen in **Fig. 2.1** and **Fig. 2.2.**

Fig. 2.1 Relative size of PW-4090 engine to Boeing737 aircraft fuselage. Courtesy United Airlines [6]

If it is thought the gas-turbine engine with case and nacelle cowling, it is known that there is an area where noisy, hot and high vibration exists and here engine controls and engine-powered services are located [6].

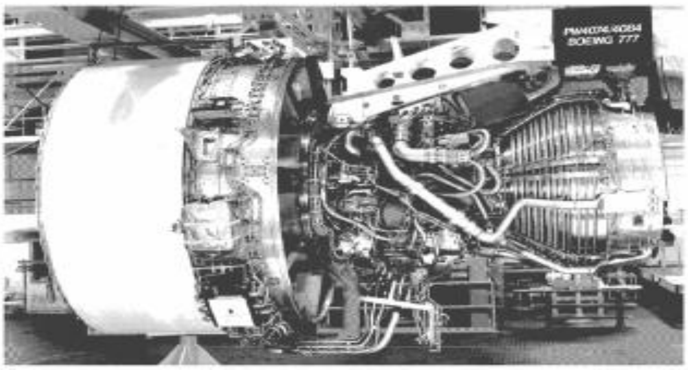

Fig. 2.2 Modern aeronautical gas turbine engine. Courtesy Pratt & Whitney [6]

The problem is how to control the large changes in geometry between adjacent rotor/stator components from cold-build to operation. The challenge is to provide geometric control while maintaining efficiency, integrity and long service life (e.g., estimated time to failure or maintenance, and low costs).

Engine seal clearance must accommodate large changes in thermal and centrifugal loadings. The clearance between the rotor tip and the case differs during take of, climb and cruise condition. More information about the dramatic effect of clearance control via applied cooling to the casing can be found in turbomachine interface sealing [6].

Changing sealing parameters can change the dynamics of the entire engine [6]. Therefore, designers must be very careful with the parameters because these effects cannot be always positive.

2.1.2 Sealing Benefits

Performance issues are strongly related to engine clearances. Improvement of the sealing technologies provides to increase energy saving in high ranges. If it is wanted to understand this effect clearly, it should be looked at some numbers about the relationship between sealing and the costs. Therefore below, some data were taken from different researches [7] to show this effect.

- Ludwig determined that improvements in fluid film sealing resulting from a proposed research program could lead to an annual energy saving, on a national basis, equivalent to about 37 million barrels (1.554 billion U.S. gallons) of oil or 0.3 percent of the total U.S. energy consumption (1977 statistics).
- In terms engine bleed, Moore cited that a 1 percent reduction in engine bleed gives a 0.4 percent reduction in specific fuel consumption (SFC), which translates into nearly 0.033 (1977 statistics) to 0.055 (2004 statistics) billion gallons of U.S. airlines fuel savings and nearly 0.28 billion gallons worldwide (2004 statistics), annually.
- In terms of clearance changes, Lattime and Steinetz [7] cite a 0.0254 mm (0.001 in.) change in HPT tip clearance, decreases SFC by 0.1 percent and EGT (exhaust gas temperature) by 1 °C, producing an annual savings of 0.02 billion gallons for U.S. airlines.
- In terms of advanced sealing, Munson et al. estimate savings of over 0.5 billion gallons of fuel.
- Chupp et al. estimated that refurbishing compressor seals would yield impressive improvements across the fleet ranging from 0.2 to 0.6 percent reduction in heat-rate and 0.3 to 1 percent increase in power output. For these large, land-based gas turbines, the percentages represent huge fuel savings and monetary returns with the greatest returns cited for aging power systems [7].

2.1.3 Seal Types and Locations

For seal types and locations industrial and aero-turbomachines have many differences like fan and combustor. However aeroengines derive a large portion of their efficiency through the bypass fan and have inline combustors, industrial engines are not bound by flight requirements [6].

Actually, core requirements for both engines are similar but the materials have different restrictions. Therefore, sealing types such as labyrinth, brush, face and mechanical seals etc. all of them need special interface materials and coatings.

Key sealing locations for the compressor and turbine in an industrial engine are given in **Fig. 2.3** and **Fig. 2.4.**

Here just the locations are shown to understand and to have an opinion where the sealing in turbomachines is. More information about seal location and the properties are given in [7].

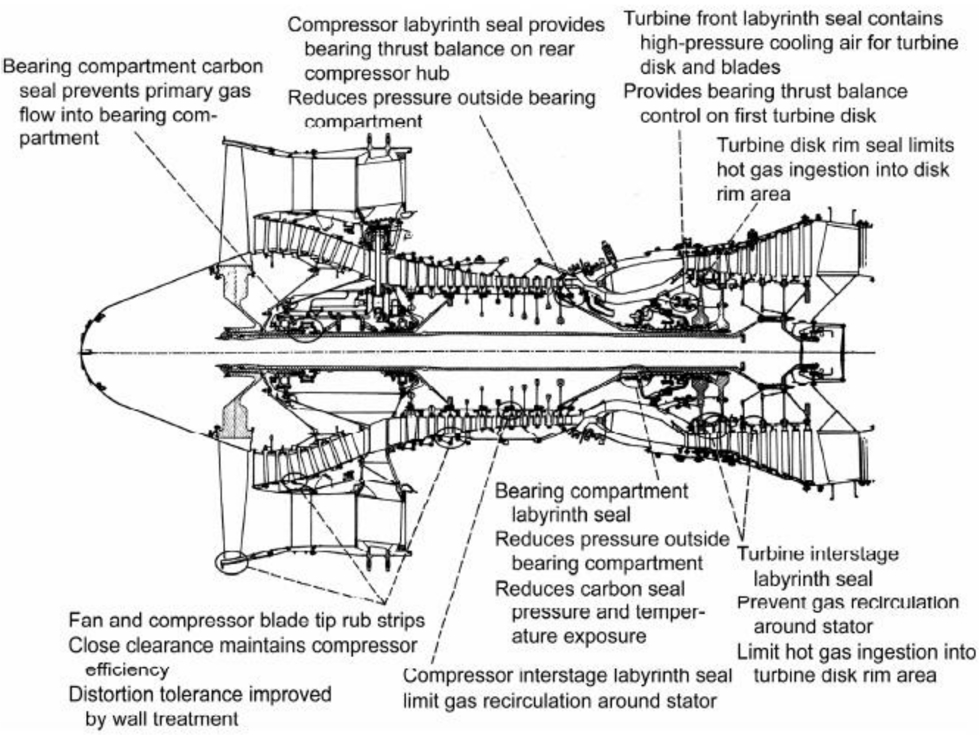

Fig. 2.3 Key aero-engine sealing and thermal restrain locations [7]

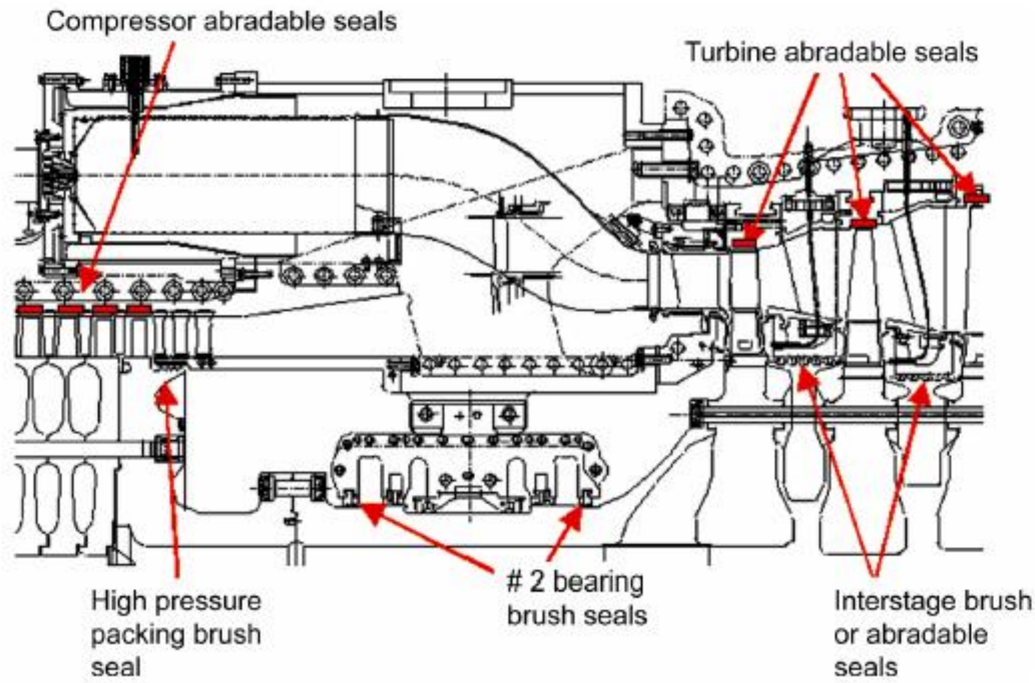

Fig. 2.4 Advanced seals locations in a frame 7EA gas turbine [6]

2.1.4 Materials and Environmental Conditions

The development of the material technology gives a chance to work with the high operating temperatures for the turbine engines components. Especially Ni-based single crystal alloys and the coatings allow reaching high temperatures. Consideration of the thermal and pressure a profile, in the sealing technology is worked with materials from steel to super alloys coated with metallics and ceramics.

Figure 2.5 and **2.6** show the schematic of the thermal requirements and suggested types of sealing materials that can be used at these locations.

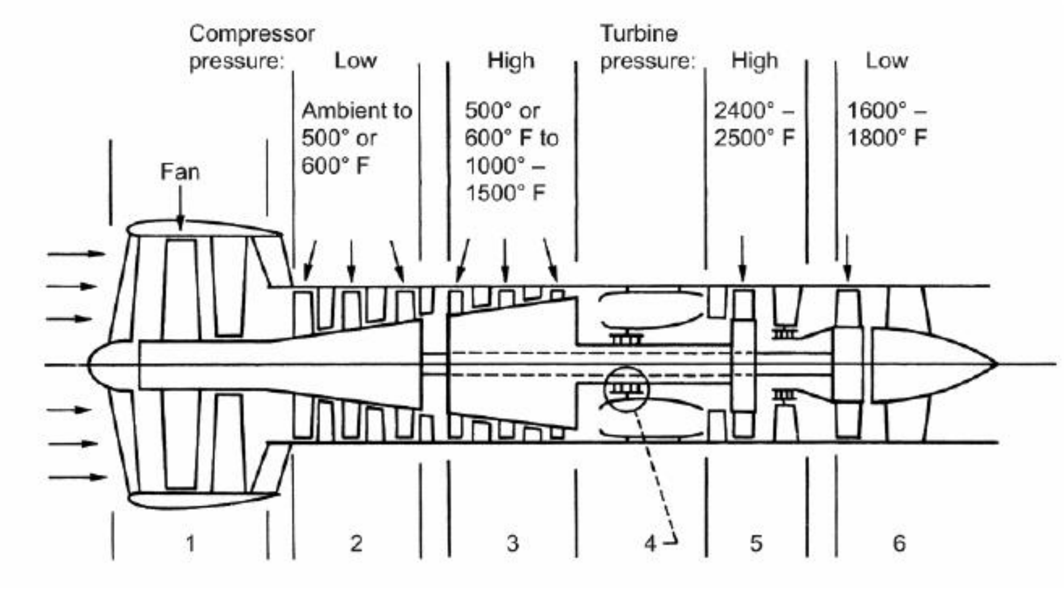

1, silicone rubber, aluminum honeycomb, epoxy; 2, sprayed aluminum, sprayed nickel-graphite, silicone rubber, fibermetal; 3, Hastelloy-X fibermetal, sprayed nickel-graphite, sprayed Nichrome with additives; 4, labyrinth seals, silver braze, fibermetal, honeycomb; 5, cast superalloy (cooled), sintered high-temperature metals, ceramics; 6, superalloy honeycomb.

Fig. 2.5 Summary of engine operating environments and typical adradable seal materials [7]

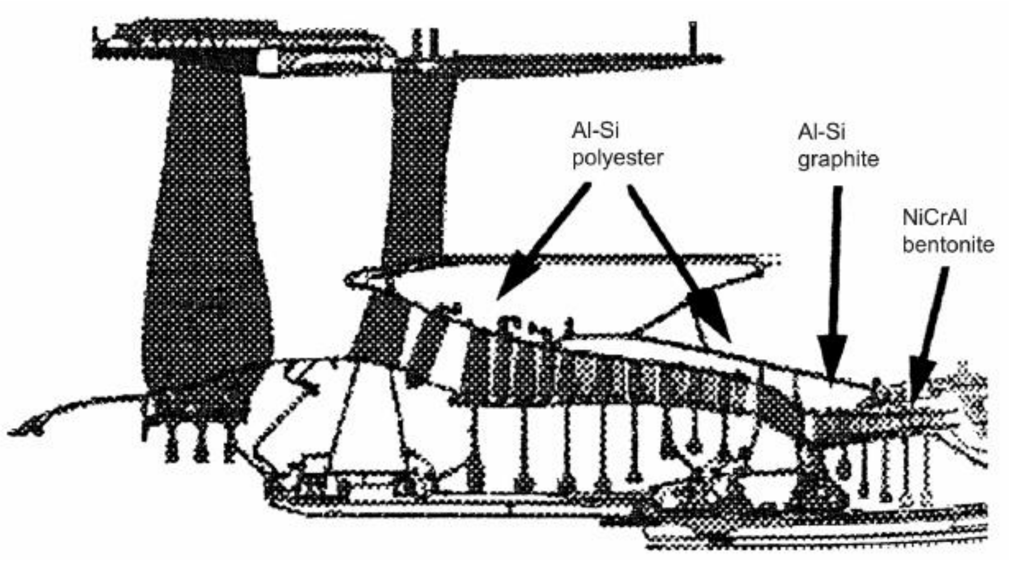

Fig. 2.6 The intermediate and high-pressure compressor of a modern gas turbine engine showing where the Al-Si and Ni-base abradable sealing are used [7]

In this section, it will be no more discussed the materials and the properties. The aim was to give general information about it. Every sealing material has different operating temperature and pressure rate, the detailed information about it can be found in every sealing type research.

2.2 Static Sealing

The sealing in static or slow interface relative movement locations in turbomachinery includes the interfaces or junctions between the stationary components. It compromise also the internal cooling flow path to minimize or control parasitic leakage flows between turbine components.

At the static interface locations, sealing increases the turbine efficiency and output. The main gas-path temperature profile is also improved. Metallic Seals, Metallic Cloth Seals and Cloth and Rope Seals are developed for the static sealing and in the next sections, they will be shortly expressed.

2.2.1 Metallic Seals

For some locations in turbine, rubber and polymer seals are not suitable for higher temperature and pressure environment. Therefore the metallic seals are used in these locations.

The range of applications in turbomachinery is quite wide, so it is needed multiple configurations for the metallic seals such as the O, C, and E-type cross section. The type of the seal that is best suited for a particular application depends on operating variables such as temperature pressure, required leakage rate, flange separation, fatigue life and the load available to seat seals.

2.2.2 Metallic Cloth Seals

In turbomachinery applications with significant relative motion, some metallic seals are inadequate for sealing (rigid metal strips, feather seals etc.). Therefore, the thickness of the seal strips need to be reduced.

Cloth seals are formed by combining thin sheet metals (shims) and layer of densely woven metal cloths [7]. The shims prevent through leakage and provide structural strength with flexibility. As well as that external cloth layers add sacrificial wear volume and seal thickness without adding significant stiffness.

2.2.3 Cloth and Rope Seals

Rope and gasket seals can be used in various locations in turbomachinery. **Table 2.1** lists the various materials being used. However, the temperature of the aircraft engine turbine and industrials systems temperatures continue to climb to meet aggressive cycle thermal efficiency goals [7].

TABLE 1.—GASKET/ROPE SEAL MATERIALS

Fiber Material	Maximum working temperature (°F)	°C
Graphite		
Oxidizing environment	1000	540
Reducing	5400	2980
Fiberglass (glass dependent)	1000	540
Superalloy metals (depending on alloy)	1300–1600	705–870
Oxide ceramics (Thompkins, 1955)[18]	1800[a]	980
Nextel 312 (62% Al_2O_3, 24% SiO_2, 14% B_2O_3)	2000[a]	1090
Nextel 440 (70% Al_2O_3, 28% SiO_2, 2% B_2O_3)	2100[a]	1150
Nextel 550 (73% Al_2O_3, 27% SiO_2)		

[a] Temperature at which fiber retains 50 percent (nominal) room temperature strength

Table 2.1 The summarize of gasket/rope seal materials [7]

In advanced material systems, there are some materials, including monolithic/composites ceramics, intermetallic alloys (i.e. nickel aluminide), carbon-carbon composites. They are able to meet aggressive temperature, durability and weight requirements. In the high temperature locations of the system to incorporate these materials, designer must overcome material issues. These are the differences in thermal expansion rates and lack of material ductility [7].

2.3 Dynamic Seals

2.3.1 Blade Tip Sealing

If it is looked at the flow field at the tip of the blades for the compressor and turbine, at the leading edge the flow is forced out and around the stagnation region, then joins with the primary leakage zone. After that it extends across the passage toward the low pressure side and opposing the rotational velocity. Because of this, blade tip flows and ensuring vortex patterns lead to flow losses, instabilities and passage blockage. Without proper sealing, the flow field can be reversed, resulting in compressor surge and possible fire at the inlet.

Based on the problematic issues which it is mentioned, the management of blade tip leakage is important to improve engine designs in several ways. The compressor efficiency, stall/surge margins and the engine operability are improved by reducing compressor blade tip leakage. Maintaining tighter clearances over the life of the engine addresses a key observation that 80-90% of engine performance degradiation is caused by blade tip clearance increase. In a limited number of commercial engines, blade tip clearance control is used. Blade tip clearance control is performed by preferentially cooling the turbine case during cruise operation [3, 7].

2.3.2 Abradable Seals

In the sealing technologies, researchers recognized the need for adradable materials for blade tip and vane sealing. Adradable seals have been in use in aviation gas turbines since the late 1960s and early 1970s. Although low energy costs, materials and long cycle time have in the past limited applications of abradable seals in land based gas turbines, current operation demands enhanced heat rate and reduced costs. After increasing fuel prices and advanced in materials to allow extended service periods, abradable seals are gaining the popularity within the power generation industry [7].

This type of sealing reduced the blade tip clearance. Abradable seal materials are worn in the rotating blade during the service. It is placed on the stationary shroud or casing opposite the rotating blade tips to reduce clearances with minimum risk to turbine components during rubs. The applying an abradable material reduces effectively clearance for often-encountered casing out of roundness and rotor lateral movement. A thermally sprayed coating is applied to stage 1 E-Class gas turbine shrouds to reduce tip clearances and improve turbine performance up to 0.8%. Honeycomb is used as an abradable seal in the stage 2 and/or 3 of E-Class turbines with performance benefits up to 0.6%. Efforts are continuing to develop abradable materials for these turbine locations with increased service life.

Schematics of three types of abradable materials with associated incursion types are illustrated in **Fig. 2.7** for outer air-blade tip sealing interface in a compressor.

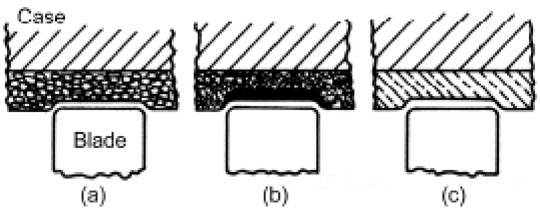

Fig. 2.7 Illustration of types of materials for interface outer air sealing (a) Adradable(sintered or sprayed porous materials.) (b) Compliant (porous material). (c) Low shear strength (sprayed aluminum) [7]

Abradable seals can be classified according to their temperature capability. These are low temperature, generally for LP compressors, Mid-range for LP and HP compressors, and high temperature for HP turbines. On the other hand, they can be also characterized by their method of application and they are casting for polymer abradable materials, brazing or diffusion bonding for honeycomb and/or fiber metals (porous fiber metal structures) and thermal spray coatings for a large range of powdered composite materials [3].

Finally it can be said that abradable seal materials have a big role to decrease the operating blade tip clearance. Without abradable seals, the cold clearances between blade or bucket tips and shrouds must be large enough to prevent significant contact during operation. Use of abradable seals allows the cold clearances to be reduced with the assurance that if contact occurs, the sacrificial part will be the abradable material on the stationary surface and not the blade or bucket tips. Also, abradable seals allow tighter clearances with common shroud or casing out-of-roundness and rotor misalignment.

For more information and detailed analyses of abradable sealing technologies see [7].

2.3.3 Carbon Face Seals

Face seals are classified as mechanical seals. They are pressure balanced contact or self-acting seals. The important components are the primary ring (stator) or nosepiece, seat or runner (rotor), spring or bellows preloader assembly, garter or retainer springs, secondary seal and housing. For the face seal, the geometry of the ring or nosepiece becomes critical. The forces due to system pressure, sealing dam pressure and the spring or bellows must be properly balanced and stable over a range in operating parameters for the successful face sealing. These operating parameters are pressure, temperature, surface speed [7].

Face seals can be seen in bearing locations in turbine engines and auxiliary power units. The face seals with carbon graphite have high corrosion resistance, natural lubrication and low leakage. It can be used for the seal pressures up to 1 MPa. Some of the carbon face seals are showed in **Fig. 2.8.**

Fig. 2.8 Examples for carbon face seals [31]

Low costs of face seals make them an alternative to more expensive labyrinth seals. It is practical and less costly especially in advanced aircraft engines [3, 7].

For inserting the carbon into mechanical seals there are two options. One of them is called monolithic face seal and the other called composite face seals. The composite face seals have some advantages over the monolithic types such as cross section. Because carbon part can have a smaller cross section if the composite seals are used. It has a big role in material homogeneity. It is easier to impregnate smaller part and eliminate unwanted air pockets and making it better heat conductor. Carbon has a better compression feature then tension feature. The carbon face is kept by metal holder in compression. On the other hand, the metal holder acts as a heat sink and carries unwanted heat away from the face seal. The disadvantages of using carbon/metal composite include differences in thermal expansion of materials. The carbon part can loosen in the holder and start to leak or spin.

Another problem with using face seals is coking and blistering. Coking appears during sealing oil environments. And if there is a large diameter to seal, the problems occur. According to Carlile et al. tolerance control makes the costs rise significantly. To overcome coking problem and oil odour in the cabin, carbon face seals were replaced with ceramic ring seals and the seal operating life was also significantly increased.

For more details on carbon face seals refer to [3, 33].

2.3.4 Oil Seals

The other type of sealing is oil seals. There are two types of sealing that are used in oil seals. They are radial face seals and the ring seals. Gas turbine shaft seals are used to restrict leakage from a region of gas at high pressure to a region of gas at low pressure. A common use of mechanical seals is to restrict gas leakage into bearing sumps. Oil sealing of bearing compartments of turbomachines is difficult. A key is to prevent the oil side of the seal from becoming flooded. Still, oil-fog and oil-vapour leakage can occur by diffusion of oil due to concentration gradients and oil transport due to vertical flows within the rotating labyrinth-cavities (crude distillation columns). Bearing sumps contain an oil-gas mixture at near-ambient pressure, and a minimal amount of gas leakage through the seal helps to prevent oil leakage and maintains a minimum sump pressure necessary for proper scavenging. Bearing sumps in the HPT are usually the most difficult to seal because the pressure and temperatures surrounding the sump can be near compressor discharge conditions.

For more information about the oil seals, refer to [7].

2.3.5 Labyrinth Seals

Labyrinth seals are the most commonly used flow path seals over turbine engine history. Labyrinth seals and their sealing principles are commonplace in turbomachinery and come in a variety of configurations. The most used configurations are straight, interlocking, slanted, stepped and combinations. By their nature labyrinth seals usually mounted on the rotor, are clearance seals that can rub against their shroud interface, such as abradables and honeycomb [7]. They permit controlled leakages by dissipation of flow energy through a series of sequential aperture cavities (as sequential sharp edge orifices) with minimum heat rise and torque. The speed and pressure at which they operate is only limited by their structural design.

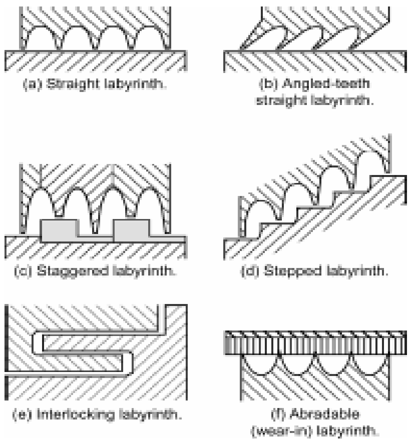

Fig. 2.9 Generalized labyrinth seal configurations [7]

Figure 2.9 shows some seal configurations. Principle design parameters include: clearance and throttle (tooth or knife) and cavity geometry and tooth number. The clearance is set by aerothermomechanical conditions that preclude contact with the shroud allowing for radial and axial excursions. The throttle tip is as thin as structurally feasible to mitigate heat propagation through the throttle-body into the shaft with a sharp leading edge (as an orifice) and is the primary flow restrictor. The angle at which the flow approaches the throttle is usually 90° but slant throttles, into the flow, are more effective seals [7].

Labyrinth seals are clearance type seals and because of this they have high leakage rates. In time increase the leakage. Labyrinth seals are used as shaft seals, turbine rim seals, and as inner air seals sealing the vane-to-drum inter-stage locations [3].

2.3.6 Finger Seals

The finger seal is a relatively new seal technology developed for air-to-air sealing for secondary flow control and gas path sealing in gas turbine engines. It can be easily used in any machinery to minimize airflow along a rotating or non-rotating shaft. Measured finger seal air leakage is 1/3 to 1/2 of conventional labyrinth seals. Finger seals are compliant contact seals. The power loss is similar to that of brush seals [7]. It is reported that the cost of finger seals are estimated to be 40 to 50 percent of the cost to produce brush seals.

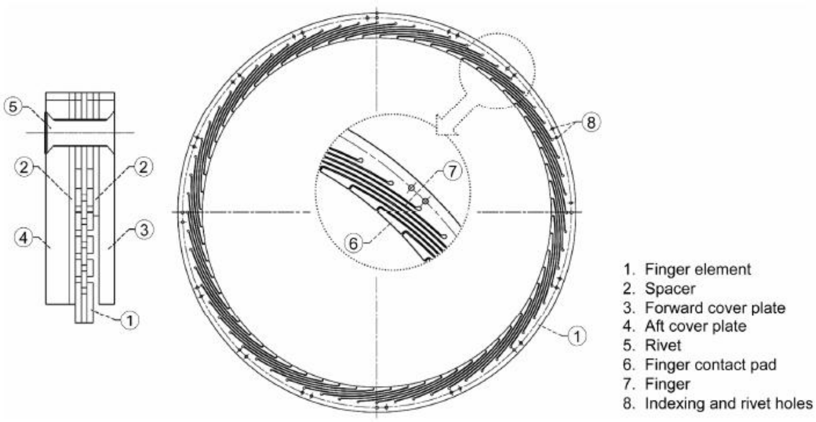

Fig. 2.10 Finger seal and detailed components [7]

The finger seal is comprised of a stack of several precisely machined sheet stock elements that are riveted together near the seal outer diameter. Each finger element has been machined to create a series of slender curved beams or fingers around its inner diameter. The finger elements are alternately indexed so that the fingers of one element cover the spaces between the fingers on the adjacent element. The flexible fingers can bend radially to accommodate shaft excursions and relative growth of the seal and rotor resulting from rotational forces and thermal mismatch. The seal is made of sheet AMS5537, a cobalt base alloy that has good formability, excellent high temperature properties, and displays excellent resistance to the hot corrosive atmospheres encountered in jet engine operations [3]. Finger seal and detailed components can be seen in **Fig. 2.10**.

2.4 Advanced Seal Designs

In the seal technologies aim is always definite: to improve the efficiency of the engine. It is tried to provide also to avoid leakages in the turbomaschines. Therefore, there are always many researches to develop or to optimize the sealing technologies.

In advanced seal designs, some of the seal technologies and sealing methods are: normal/non-contacting finger seals, leaf and wafer seals, hybrid brush seals, aspirating seals, micro-dimple surfaces, wave interfaces, seal bearing, compliant foil seal, deposits control, active clearance control(ACC) etc.

In this section it is given just the names of them. For the detailed information, refer to [7].

2.5 Life and Limitations

In the sealing technology, life and limitations are the important parameters. Because these methods are not cheap and it is not easy to apply. The designers must be very carefully and they must consider whole design parameters at the same time. System design conditions for sealed controlled component cooling are driven by compliance to regulatory agencies, reliability and safety standards. The mean time between failures (MTBF) is highly dependent on the thermal loading and the aero-engine and flight operations profile.

Zaretsky et al. applied Weibull-based life and reliability analysis to rotating engine structures. When limits are placed on stress, temperature, and time for a component's design, the criterion that will define the component's life and thus the engine's life will be either high-cycle or low-cycle fatigue.

Knowing the cumulative statistical distribution (Weibull function) of each engine component is a prerequisite to accurately predicting the life and reliability of an entire engine. **Table 2.2** shows how some of the hot section component lives correlate to aero-engine maintenance practices without and with refurbishment, respectively. That is, it can be reasonably anticipated that at one of these time intervals, 5 percent of the engines in service will have been removed for repair or refurbishment for cause.

	Service life (hr)	Total life with repair (hr)
Combustor	9,000	18,000
HPT rotating structure	18,000	36,000
HPT blading	9,000	18,000
Remainder of engine	--------	36,000

Table 2.2 E3 Engine flight propulsion system life based on 1985 technology and experience [3]

There are not so much data for seals and their functional life and for basic materials in the open literature. There are some approaches to determine life of the components. Some of them are the Weibull-based analyses or MTBF. For the more detailed information, refer to [3, 7].

3. Brush Seals

3.1 History and Development

Brush seals have a large history. They have been successfully applied in rotating machinery since the 1980s. But if it is gone a little earlier, it can be reached the 1955. There was the first attempt to replace labyrinth seals with brush seals by General Electric (GE). GE tried to use this technology in J-47 engine which was the better version than J-35 and was tested firstly in May 1948. But this attempting was unsuccessful. After that Rolls Royce managed to apply brush seals in the 80's in demonstrator engines. Then in 1987, RB-199 engine was produced with installed brush seals. IAE V2500 is an engine certified in 1987. It was, for several years, the only production engine with brush seals [3].

In 1988 Ferguson [7] has published his research on brush seals. There has been an ever increasing interest in their usage and in the mechanisms that control their performance. The main reason behind this was the opportunity of using them as a direct replacement for labyrinth seals. Because it gives a substantial improvement in leakage characteristics. It was recognized that if this was possible, particularly in the more arduous sealing positions of a gas turbine, significant improvements in cycle efficiencies could be achieved [9]. Although a brush seal looks very simple in its design, research and aero engine experience has shown the complex nature of the flow fields and mechanics. Braun et al. [22] showed that many different flow features of through flow exist in a seal [11].

As a result, the brush seal is the first simple, practical alternative to the labyrinth seal, and it gives performance improvements.

3.2 Construction and Model

A brush seal is a circular seal and it is used for fluid sealing in rotating machinery. It is common used in gas turbines between rotating and stationary parts. It consists of three main components: bristle pack, front plate and backing plate. Simply a schematic diagram of brush seal can be seen in **Fig. 3.1**.

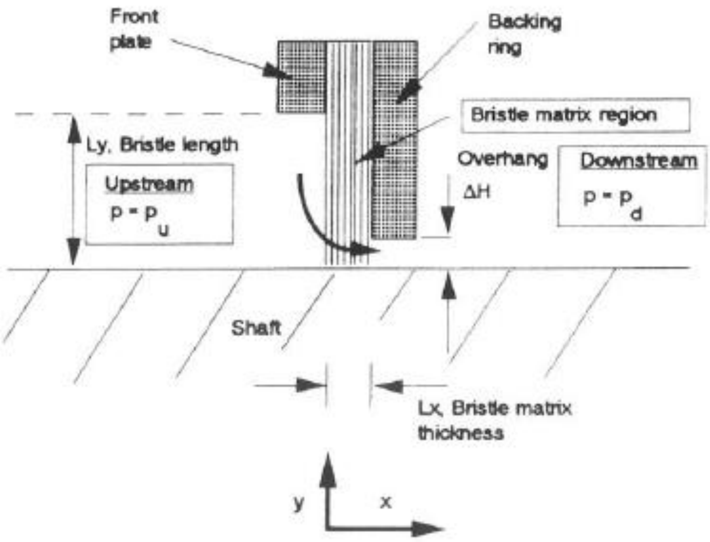

Fig. 3.1 A schematic diagram of a brush seal [1]

Brush seal construction is relatively simple. It is here important that the well ordered layering of fine-diameter bristles into a dense pack. Because this dense pack compensate the difference or it can be also said distance between inside and outside diameters. This pack is sandwiched and in some designs welded in some designs mounted without welding between a backing plate (downstream side) and front plate (upstream side). If it is welded, the weld on the seal outer diameter is machined to form a close-tolerance outer diameter-sealing surface to fit into a suitable housing [7].

The major component of the seal is a pack of bristles with the thickness ***B***. The usual amount is 1200 bristles per centimeter circumferential of the seal. The individual bristles are arranged at a lay angle $\boldsymbol{\theta}$ to the tangential direction. The bristle lay angle is defined as the angle between the tangential direction and the direction of the bristles. This arrangement allows the bristles sufficient freedom to follow any rotor excursion. **Table 3.1** shows some typical geometric values for brush seals and in **Fig. 3.2** lay angle can be seen.

Bristle diameter	$\sim 70\ \mu m$
Number of bristles	$\sim 100 - 200\ 1/mm$
Bristle length	$\sim 7 - 10\ mm$
Backing plate gap	$1 - 2\ mm$
Lay angle	$\sim 45^o$

Table 3.1 Typical geometric values for brush seals

The backing plate supports the bristles. In this way, bristle pack can carry the pressure load. The backing plate prevents the bristles from deflections in axial direction and blowing outwards. Clearance between the backing plate and rotor is important and it should be high enough to accommodate any excursion due to the vibrations or centrifugal and thermal growth.

The bristles extend beyond radially inward or outward. To accommodate anticipated radial shaft movements, the bristles must bend. Therefore the wires are oriented at an angle. Thus the bristles can be bended without buckling.

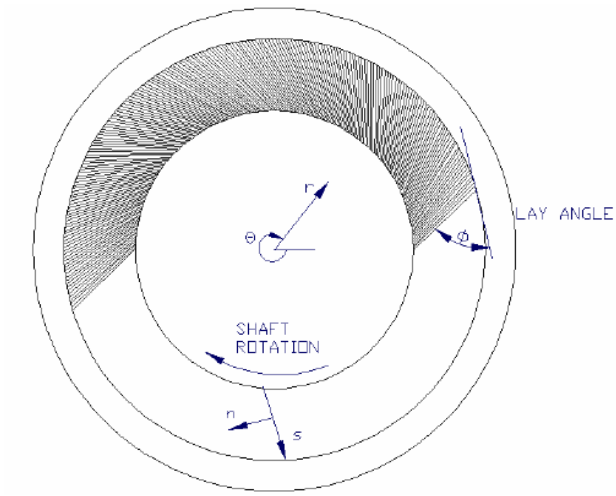

Fig. 3.2 Brush seal front view

The lay angle here is one of the most interesting parameter. It is an angle at which bristles are tilted towards the shaft. The standard value is between 45^o-55^o but usually it is taken 45^o in the direction of the shaft rotation. If a contact with rotor occurs, bristles are pushed away from the shaft. As we said before, they are designed to bend and this angle prevents bristles from buckling, which would appear if the bristle were aligned radially. On the other hand, the angle influences the bristle wearing resistance and improves the sealing.

The lay angle of bristle in the direction of rotor rotation gives us another advantage. The flexible bristle pack tolerate the rotor excursions due to operation conditions, such as vibration, centrifugal and thermal growth, with less wear compared to the other sealing applications [21].

Under the pressure load, the behavior of the bristle pack characterizes the performance of the brush seal. This performance can be explained with the leakage and life, and these two performance criteria depend on the clearance between bristle tips and the rotor surface. One of the main advantages of a brush seal is that we can reach the minimum clearance between the rotor and stator; it means rotor and the bristle tips. The brush seal ring fits on the rotor surface with or without small clearance. Because in some designs the bristle tips touch the rotor. But the decreasing clearance minimizes the leakage.

But this time it shortens the seal life. Because if the clearance is so small or there is no clearance, then increase the wear between bristle tips and rotor surface.

Seal dynamics and performance are affected by the flow and the pressure fields in bristle pack. There are many researches on this area. One of them is the research by O'Neill at al. [21]. He reported bristle instability caused by momentum of the leakage flow hitting the bristle pack. The bristle pack forms a complex porous structure which is blocking the flow path. When the flow comes through bristles, the bristle move under the balance of elastic forces, aerodynamic forces and frictional forces among bristles, between the bristles and backing plate.

There are two main issues appearing from the balance of these forces. The bristles get tighter as pressure load pushes them against the backing plate. At the same time the airflow moves radially downward through the bristle pack causing the bristles to be driven towards the rotor and change the lay angle. It is called blow-down effect. Blow-down tends to close clearance with the rotor surface, yet it increases the bristle tip wear for excessive pull down interference.

To deal with this problem, it is possible to incorporate a flow deflector upstream of the bristle pack, as seen in **Fig. 3.3.** This solution is described in detail in the article by Short [26] and Aksit [14].

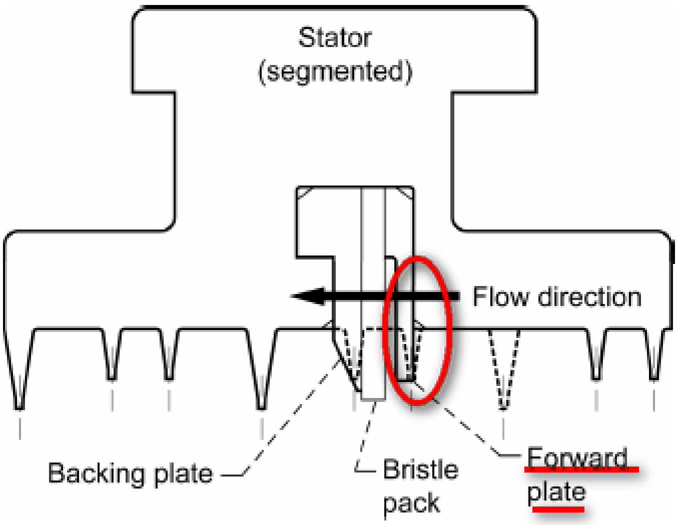

Fig. 3.3 Typical brush seal configuration and geometric features [7]

Another issue is pressure-stiffening effect. When the aerodynamic forces cannot overcome the interval friction within the bristle pack, this is called bristle hang-up. It takes place when the bristle pack is compressed and pushed against the backing plate. Friction between bristles themselves increases as well as between bristles and backing plate. Thus seal flexibility is reduced significantly. Effect grows proportionally with the growth of pressure difference. If this effect is seen, it can be understood that it is important to design a pressure-balanced bristle pack. It is possible to deal with this problem by adding a relief in the backing plate [26].

There is also a hysteresis issue for increasing versus decreasing pressure loading during the operation. This effect decreases brush seal effectiveness in this case bristles are stuck at displaced position after, for example rotor excursion. After that they do not return to their previous position. It creates a gap and this result to higher leakage flow.

The locations of the seal elements are given in chapter 2 generally. But if it is given a little more information about the brush seal placements, typical locations for brush seals at rotor shaft are end packing locations and interstage shaft seal. For example in steam turbines a typical high pressure section may have 8-12 turbine stages. The most common brush seal application would be one brush at each interstage location, and 3-6 brush seals at end packing locations [3]. As seen in **Table 3.2** the performance benefit of brush seals in steam turbines makes them a significantly worthwhile investment in the majority of utility and industrial units.

	Utility ST	Industrial ST
Interstage	0.5 - 1.2 % HP section efficiency 0.1 - 0.2 % unit heat rate	0.2 - 0.4 % efficiency
End Packing	0.1 - 0.2 % unit heat rate	0.4 - 0.8 % efficiency
Bucket Tip	0.5 - 1.0 % HP section efficiency 0.1 - 0.2 % unit heat rate	0.7 - 1.1 % efficiency

Table 3.2 Performance benefits [3]

The pressure drop across interstage seal lay averagely between 0.68MPa – 2.7MPa.

Rotordynamics is one of the important parameter to consider. Up to this consideration, it is decided how many seals are applied and at which locations, and with which level of assembly clearance/interface. If it is also here talked about the installation, brush seals can be installed in series and it is possible to put more than one seal next to each other to obtain some working parameters. These include improving of reliability of critical engine components, distribution of the pressure drop per brush and mitigation of wear. For example, dual brush seals leakage factor is approximately 2.5 times smaller than in comparable labyrinth seals [7]. On the other hand, addition of lubricant to the bristles reduces the leakage by 2.5 times when compared with non-lubricated bristles [3].

Finally it is here given according to NASA report [2], benefits of brush seals over labyrinth seals include:

- Reduced leakage compared to labyrinth seals (upwards of 50 percent possible).
- Accommodate shaft excursions due to stop/start operations and other transient conditions. Labyrinth seals often incur permanent clearance increases under such conditions, degrading seal and machine performance.
- Require significantly less axial space than labyrinth seal.
- More stable leakage characteristics over long operating periods.

3.3 Design Considerations

Many design factors must be considered to properly design and specify brush seals for an application. An iterative process must be followed to satisfy seal basic geometry, stress, thermal (especially during transient rub conditions), leakage, and life constrains to arrive at an acceptable design. In this section, it is here given a summary of some researches about some of these parameters and their effects [3].

3.3.1 Material Selection

The wear resistance is the most important parameter for the materials. The materials in rubbing contact in brush seal installations must have sufficient wear resistance to satisfy engine durability requirements. Furthermore the seal material must have acceptable creep and oxidation properties. There are two kinds of bristles materials: metallic and non-metallic materials.

Brush seal wire bristle range in diameter from 0.071mm (for low pressure) to 0.15 mm (for high pressure). In the metallic materials, the most commonly used material for brush seals is the cobalt-based alloy Haynes 25 based on its good wear and oxidation characteristics. This alloy is a Cobalt-Nickel-Chromium-Tungsten alloy that combines excellent high temperature strength with good resistance to oxidizing environments up to 1253 K for prolonged exposure. In **Table 3.3** some chemical composition of wire sampled can be seen. It has also excellent resistance to sulphidation. Haynes 214 is a Nickel-Chromium-Aluminium-Iron alloy that is principally intended for use at temperatures of 1228 K and above it. It exhibits resistance to oxidation that far exceeds virtually all conventional, heat resistance wrought alloys at these temperatures. IX750 composition is a Nickel-Chromium alloy made precipitation hardenable by addition of Al and Ti, having a creep-rupture strength at high temperatures to about 973 K [3]. Results of experiments done at NASA Lewis Research Centre show the influence of different material compositions on bristle durability. **Table 3.4** shows some wear test results.

	Co	Ni	Cr	Fe	W	Others (<6 wt. %)
H25	51	10	20	3	15	Mn, Si, C
H214	-	75	16	3	-	Mn, Si, Al, C, B, Zr, Y
IX750	0-1	70	14-17	5-9	-	Ti, Al, Nb, C

Table 3.3 Chemical composition of wire sampled (wt. %) [3]

The brush seals are generally run against a smooth, hard face coating to minimize shaft wear and the chances of wear-induced cracks from affecting the structural integrity of the rotor. The usual coatings selected for aircraft applications are ceramic, including chromium carbide and aluminium oxide.

Non metallic brush seals are also on investigation. High speed turbine designers try to replace labyrinth seals with brush seals in bearing sump locations. But there were some problems like coking (carburization of oil particles at excessively high temperatures), metallic particle damage of precision rolling element bearings, and potential for fires. But with applying the aramid bristles for certain bearing sump locations, development efforts have found [7]. The advantages of the aramid bristles include stable properties up to 150 ^{o}C operating temperatures, negligible amount of shrinkage and moisture absorption, lower wear than Haynes25 up to 150 ^{o}C, lower leakage, and resistance to coking.

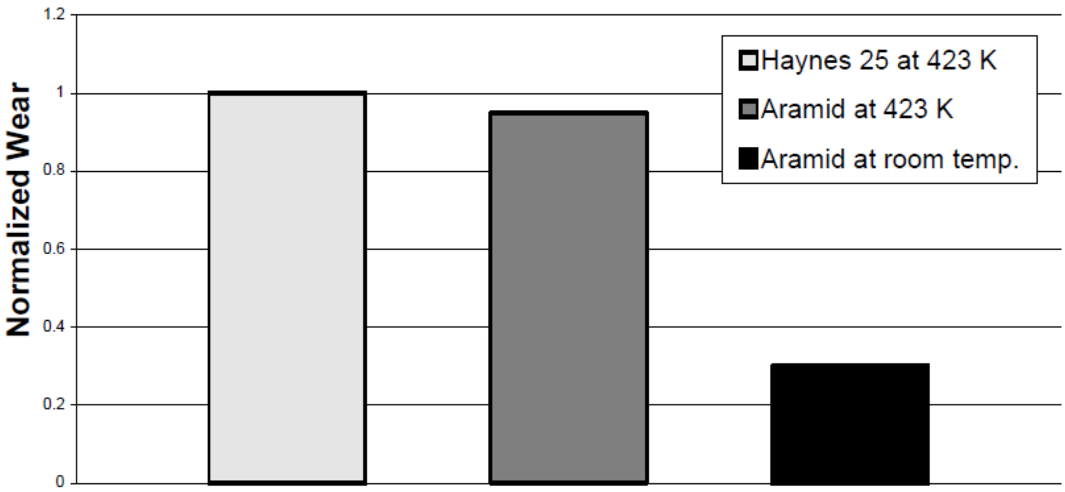

Fig. 3.4 Wear test results for Aramid and Haynes25 tufts against Ni-Cr-Mo-V. Data are normalized with wear of Haynes25 bristles at 423K [3]

Another reason of choosing a non-metallic bristle brush seal is a problem of particle generation. It is highly advised to avoid any debriefs in oil environment. Preliminary field data showed that the non metallic brush seal maintained a higher pressure difference between the air and bearing drain cavities and enhanced the effectiveness of the sealing system allowing less oil particles to migrate out of bearing.

3.3.2 Seal Fence Height

In the design procedure there is a required radial gap (fence height) between the backing plate and the rotor surface. This gap prevents to contact the backing plate with the rotor surface during any operating condition. Because it can be some dimension variations in this conditions. Therefore during the design, the knowledge of the turbine behavior, operating conditions and the design of the surrounding parts must be considered.

3.3.3 Brush Pack Consideration

Required sealing pressure differentials and life are the important parameters to choose the bristle diameters. Better load and wear properties are found with larger bristle diameters. Bristle pack widths also vary depending on application such as higher pressure or lower pressure applications.

3.3.4 Seal Stress/Pressure Capability

Pressure capacity is also one of the important design parameters. Because the overall pressure drop establishes the seal bristle diameter, bristle density and the number of brush seals in series. In a bristle pack, all bristles are essentially cantilever beams held at the pinch point by a front plate and supported by back plate. Therefore it occurs in bristle pack mean bending stress and furthermore contact stress at the bristle pack plate interface must be considered.

3.3.5 Seal Leakage

The most important parameter of a turbomachinery seal is its seal leakage behavior. Leakage characterization of brush seals typically consists of a series of tests at varying levels of bristle to rotor interference or clearance. And the behavior of the leakage mass flow versus the pressure difference must be considered. In the next chapters it will be discussed deeply and given some analyses with experimental data versus CFD modeling.

3.4 Brush Seal Flow Modeling

Actually brush seal flow modeling will be expressed deeply in the next chapter. But here it is given general information about it. Brush seal flow modeling is complicated by several factors unique to porous structures. In the bristle pack, the leakage depends on the seal porosity, which depends on the pressure drop across the seal. Flow through the seal travels perpendicular to the brush pack, through the ring formed between backing ring bore and the shaft diameter.

According to Holle et al. a flow model uses a single parameter, effective brush thickness to correlate the flows through the seal. And the variation in seal porosity with pressure difference is accounted for by normalizing the varying brush thickness by a minimum or ideal brush thickness.

According to Hendricks et al. a flow model is based on a bulk average flow through the porous media. These models account for brush porosity, bristle loading and deformation, brush geometry parameters and multiple flow paths.

A number of researchers have applied numerical techniques to model brush seal flows and bristle pressure loadings [7]. In the next chapter we will see them.

3.5 Design Types

The bristles are arranged at an angle to both the radial and circumferential directions. It is due to their geometrical properties, the bristles are flexible and withstand to rotor contact. But at this point designer encounter with some difficulties. The manufacturing of brush seal is very hard because of the small diameter of bristles. Therefore, manufacturers try to develop some new designs to make it simple.

In standard brush seal design, the bristles in the seal are joined together with the welding technology. A circumferential welding seam is applied. And the other parts such as backing plate and front plate are joined together also by welding. But the problem is here to fulfill the requirements of the design parameters. Because every single bristle needs to be safely retained, although it is very hard to work with them because of their small diameters. On the other hand, only the metallic bristles can be welded. And during the welding process, the heat can affect the bristle characteristics. Therefore, some manufacturing techniques have been found which they don’t need the welding process. **Figure 3.5** shows standard brush seal with welding technology.

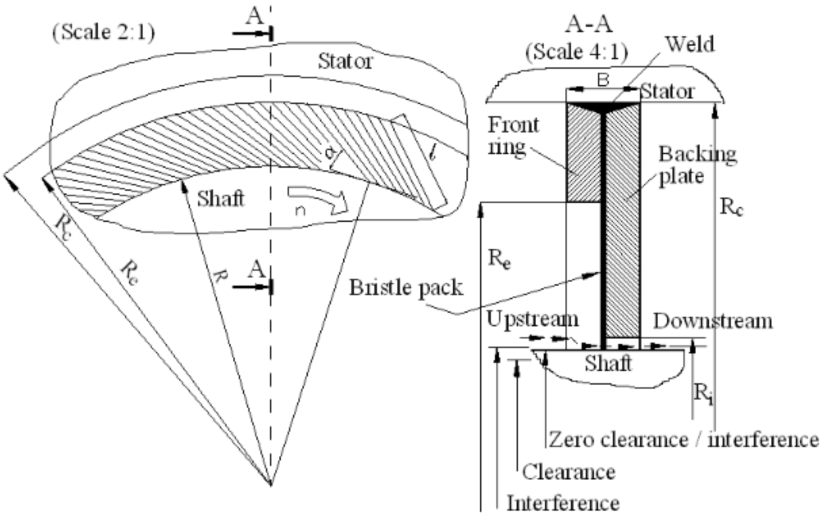

Fig. 3.5 Standard brush seal with welding technology [33]

One of the manufacturing techniques without welding is the general electric fabrication model. The brush seal patented by general electric consists of bristles that are not welded by the end tips together. **Figure 3.6** shows a cross sectional view for GE fabrication model. They extend along opposite surfaces (44) and (46). The tips (48) extend beyond the edge (50) of the carrier (42). The bristles are fitted into the grooves (52) and (54) which are formed during manufacturing process [27].

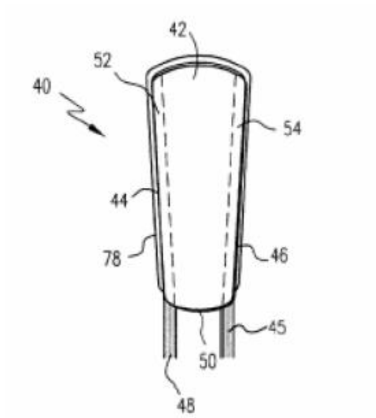

Fig. 3.6 A cross-sectional view illustrating a brush seal constructed in accordance with a preferred embodiment of patent US 6505835 [3]

The other manufacturing technique without welding is MTU brush seal design seen in **Fig. 3.7**. MTU Aero Engines calls this design “unique”. It allows creating a brush seal by joining its components without using of neither welding nor gluing processes influencing chemical and physical structure of the product. The process is using only mechanical techniques as clamping and swaging to join the parts together.

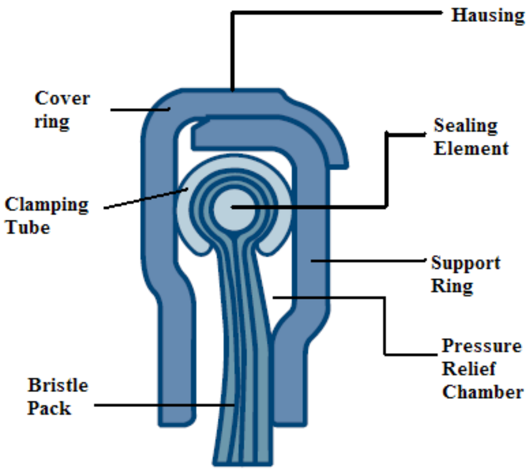

Fig. 3.7 Cross section of MTU brush seal light weight version [34]

3.6 Applications

We can categorize the application of brush seals as in aero gas turbine engines and in ground-based turbine engines.

In aero gas turbine engines, brush seals are seeing extensive service in both commercial and military turbine engines. The main characteristic of brush seal, the lower leakage, permit better management of cavity flows. Furthermore, if we compare brush seals with labyrinth seals, brush seals have significant reductions in specific fuel consumption. Allison Engines has implemented brush seals for Saab 2000, Cesna Citiation-X, and V-22Osprey. General Electric has implemented a number of brush seals in the balance piston region of the GE90 engine for the Boeing 777 aircraft. Pratt & Whitney has entered revenue service with brush seals in three locations on the PW1468 for Airbus aircraft and on the PW4084 for the Boeing 777 aircraft.

In ground-based turbine engines, brush seals are being retrofitted into ground-based turbines both individually and combined with labyrinth seals to greatly improve turbine power output and heat rate. Dinc et al [15], report that incorporating brush seals in a GE Frame 7EA turbine in the high pressure packing location increased output by 1.0 percent and decreased heat rate by 0.5 percent. To date, more than 200 brush seals have been installed in GE industrial gas turbines in the compressor discharge high pressure packing (HPP), middle bearing, and turbine interstage locations. Field data and the experience from these installations have validated the brush seal design technology. Using brush seals in the interstage location resulted in similar improvements. Brush seals have proven effective for service lives of up to 40,000hr [7].

4 Numerical Approach for Brush Seals

The flow within the bristle pack is the driving mechanism of the seal dynamics. The flow and the pressure field in close vicinity of the bristle pack have an important role to affect the performance and the seal dynamics. Therefore, dynamic behavior of the flow at turbo machinery brush seals need to be good represented and modeled. Finally the porous medium approach has been successfully used for the flow modeling in the bristle pack. It gives an opportunity to control the dynamic behaviors which affect seal performance.

There are many models with different approaches to estimate leakage and pressure load. Three of them are so famous:

- Cross flow analyses through bristles,
- Bulk flow models,
- Porous medium models.

4.1 Cross Flow Through Bristles

The first approach for flow analyses of brush seals is to analyze the flow through voids among bristles. Under the pressure load the bristles compact and form a complex structure. When the bristles dynamically move, bend, flex and twist during the operation, it is very difficult to estimate the flow paths among randomly distributed bristles. From the literature [20, 19] the flow visualization studies show that there is no uniformity of flow paths among the bristles.

The motion of bristles might concentrate in one area, while in another an interface might appear. Many flow patterns, rivering, jetting, lateral and vertical may form among the bristles. Axial pressure distribution over bristle pack is also measured as almost linear in the flow visualization studies.

The flow analyses through a uniformly positioned column of bristles give the insight for flow and pressure fields in the bristle pack only in the axial direction [21]. Staggered and in-line positions of cylindrical bristles are two types of common configurations which are studied for brush seal. Mullen et al. [3] used in-line position, while Braun and Kudriavtsev [22] solved Navier-Stokes equations for flow among a set of staggered multi row and multi column cylinders by applying a finite difference method and compared the flow field with experiments.

By these analyses, it can be estimated leakage and pressure drop through the packing thickness. But all of these analyses are two-dimensional and they neglect the radial direction, which is very important for blow-down, hang up, hysteresis, flutter etc.

On the other hand, wear occurs when the bristle tips contact the rotating part. It is a particular problem and it is important to understand the behavior of the bristle tips in such situations. Therefore 3D model of the bristle pack helps at this point. Designing a 3D model of the bristle pack includes considerations, which cannot be found in other design way. An algorithm must be applied describing bristle behavior and reaction to forces. Guardino and Chew [24] describe in general such an algorithm which created for simulation of bristles. For more information see [24, 23].

4.2 Bulk Flow Models

In this category, semi-empirical relations are developed based on flow-driven non-dimensional parameters and geometrical configurations which are the results of cross flow through bristles.

Some of the bulk flow models use the friction factor for cross flow in packed fiber and these models captured the experimental leakage trend as a function of pressure load [21].

Chupp et al. [25] has also developed one model. In this model in addition to the effective brush thickness, the pressure drop in flow across staggered tube bundles was also applied.

Holle et al. [7] use the hexagonal packing and pointed out that the use of a single parameter of effective thickness in the flow model is adequate for a bulk flow model.

Finally, it can be said that, the bulk flow models estimate the leakage mainly as a function of seal geometry and operation parameters. These models are useful for the initial design iteration.

4.3 Porous Medium Model

The other approach in brush seal flow analyses is the porous medium model which treats the whole bristle pack as a single porous medium with defined resistance to flow. It is effective and usable approach because in industrial processes the movement of gases and liquids through porous medium is very common like distillation and absorption columns, filters. Porous media approximation is used to model pressure drop at automobile radiator or a fan, flow distributors and packed beds [3].

The porous medium approach is basically solving the Navier-Stokes equation with the additional flow resistance due to friction between flow and bristles. The porous flow model gives the calculation of the pressure distribution in the bristle pack in addition to leakage and axial pressure estimations. It can be used to find pressure distribution in structural models when aerodynamic forces acting on the bristles for seal dynamic issues. This approach has been successfully applied for brush seals.

4.3.1 The Basis, Darcy

Darcy's law is an equation that describes the flow at a fluid through a porous medium. The law was formulated by Henry Darcy based on the results of experiments on the flow of water through beds of sand. He used this system, flow of water in vertical homogeneous sand filters, to supply water for the fountains in French city of Dijon. **Figure 4.1** shows his experiment set-up.

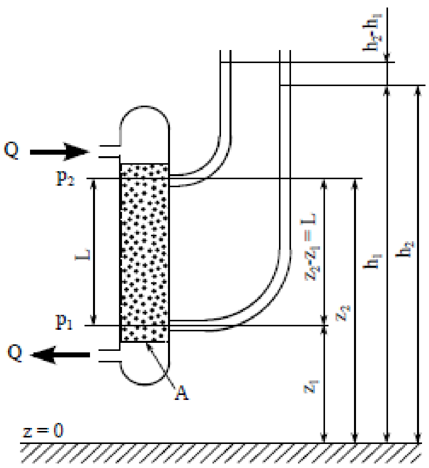

Fig. 4.1 Darcy's experiment schema [12]

From the experiment, he concluded that the rate of flow (volume per unit time) ***Q*** is proportional to the constant cross-sectional area ***A***, proportional to ***(h_1-h_2)*** but inversely proportional to the length ***L***.

Thus, as a result of the relations mentioned above gives for laminar, steady flow rate of homogenous fluid through a porous medium.

$$Q = k\,A\,(h_1 - h_2)\frac{1}{L} \qquad (4.1)$$

If the Bernoulli equations are implemented:

$$p + \frac{1}{2}\rho v^2 + \gamma h = const. \qquad (4.2)$$

$$\gamma = \rho g (specific\,weight) \qquad (4.3)$$

$$\frac{p}{\gamma} + \frac{v^2}{2g} + h = const = H. \qquad (4.4)$$

Equation 4.4 is the Bernoulli equation which is transformed to express the head.

The total head is constant along the stream line and can be measured by the stagnation pressure using a pitot-tube.

It gives Bear's equation [3] for Darcy Law.

Piozemetric head is the sum of pressure head $\frac{p}{\gamma}$ and elevation head $\boldsymbol{h}$. In a flow it can be measured through a flat opening parallel to the flow.

It describes the sum of pressure and potential energy of fluids per unit weight. Therefore $(h_1 - h_2)\frac{1}{L}$ can be interpreted as hydraulic gradient $\boldsymbol{J}$ and $\frac{Q}{A}$ as specific discharge $\boldsymbol{q}$.

$$J = (h_1 - h_2)\frac{1}{L} \tag{4.5}$$

$$q = \frac{Q}{A} \tag{4.6}$$

$$q = kJ \tag{4.7}$$

Darcy-Law can be also given in other form with the pressure and the density of fluid.

$$p_1 = \rho g(h_1 - z_1) \tag{4.8}$$

$$p_2 = \rho g(h_2 - z_2) \tag{4.9}$$

$$Q = k\,A\,(\frac{1}{\rho g}(p_2 - p_1) + (z_2 - z_1))\frac{1}{L} \tag{4.10}$$

$$z_2 - z_1 = L\,, \qquad \frac{k}{\rho g} = \frac{K}{\mu} \tag{4.11}$$

$$Q = \frac{kA}{\rho g}(p_2 - p_1 + \rho g L)\frac{1}{L} \tag{4.12}$$

4.3.2 Definition of Porosity and Some Mathematical Equations

The losses, such as pressure loss of the flow rate through the porous medium are caused mainly by the porosity. If it is assumed that, porous medium is homogeneous, at the same time fluid and solid are in thermal equilibrium, the equations describing fluid motion and energy balance in region $\boldsymbol{V}$ are as follow:

The Within $\boldsymbol{V}$: $\boldsymbol{V_f}$ is the volume occupied by fluid

$\boldsymbol{V_s}$ is the volume occupied by solid

$$V = V_f + V_s \tag{4.13}$$

And the porosity of porous medium is:

$$\varepsilon = \frac{V_f}{V} \tag{4.14}$$

To define the porous flow equations, two averaged quantities are introduced:

$$\bar{a} = \frac{1}{V}\int_{V_f} a \, dV \tag{4.15}$$

$$\breve{a} = \frac{1}{V}\int_{V} a \, dV \tag{4.16}$$

Here $\boldsymbol{a}$ is any quantity (scalar, vector or tensor).

The parameters $\bar{\boldsymbol{a}}$ and $\breve{\boldsymbol{a}}$ are referred to as pore average and value average, respectively, of the quantity $\boldsymbol{a}$**.** They are related by the equations:

$$\bar{a} = \varepsilon\breve{a}. \tag{4.17}$$

Equation 4.15 and **4.16** can be used to determine the volume-pore average velocity, pressure and temperature of the fluid, with changing just the quantity parameters.

And then it can be described the volume averaged mass, momentum and the energy equations. These equations are the generalization of Standard Darcy Equations for non-isothermal flow in a saturated porous medium. For more information see [3].

The equations in the fluid and porous medium are all solved in terms of volume-averaged quantities. Because it provides to maintain consistent boundary conditions at fluid and porous medium boundaries.

4.3.3 Permeability and Anisotropic Permeability

Standard porous medium equations treat the region as isotropic and homogenous. But the flow is not isotropic and also not homogenous in this region. If the reason is explained, isotropic medium has certain properties independent on direction and also homogenous medium has certain properties independent of position within medium. Otherwise flow is called anisotropic and heterogeneous. Bristles in brush seal represented as porous medium with the anisotropic properties. It is so because of the lay angle $\boldsymbol{\theta = 45^o}$. The bristle lay angle is defined as the angle between the tangential direction and the direction of the bristles. It has an also important role to model the behavior of the bristle pack as a porous medium. Relation between specific discharge ***q*** and the gradient ***J*** in general case of anisotropic medium can be written as:

$$q = K\,J \tag{4.18}$$

$$q_i = K_{ij}\,J_i\ (i,j = 1,2,3\ or\ x,y,z). \tag{4.19}$$

In Cartesian coordinate with Einstein's summation-convention permeability tensor ***K*** can be written in two and three dimensional form.

$$K = \begin{bmatrix} \mathrm{K_{xx}} & K_{xy} \\ K_{yx} & K_{yy} \end{bmatrix}\ and\ \begin{bmatrix} K_{xx} & K_{xy} & K_{xz} \\ K_{yx} & K_{yy} & K_{yz} \\ K_{zx} & K_{zy} & K_{zz} \end{bmatrix} \tag{4.20}$$

$K_{ij}=K_{ji}$ and the nine components K_{ij} in a three-dimensional space, or four in a two-dimensional space, define a viscous conductivity tensor. They can be written in a compact matrix form like in **Eq. 4.20**.

In the brush seal modeling, the tensor is supposed to represent the resistance at the bristles. The resistance force can be represented by the following equation:

$$\overrightarrow{F_r} = -A\eta\vec{v} - B\rho|v|\vec{v} \tag{4.21}$$

A is the viscous resistance and symmetric with principal axis in the directions normal to the bristles in the ***r-θ*** plane, parallel to the bristles and axial directions. ***B*** is the inertial resistance tensor. The governing equations are formulated in the cylindrical coordinate system (**z, r, θ**). Because basic form of the ***A*** is as follows:

$$A = \begin{bmatrix} a_{rr} & a_{r\theta} & a_{rz} \\ a_{\theta r} & a_{\theta\theta} & a_{\theta z} \\ a_{zr} & a_{z\theta} & a_{zz} \end{bmatrix} \tag{4.22}$$

The transformation of the resistance coefficients of the tensors ***A*** and ***B*** from the principal axes to cylindrical coordinate system is given for example by Bear(1988) [2].

$$A = \begin{bmatrix} a_s sin^2\varphi + a_n cos^2\varphi & (a_n - a_s)sin\varphi cos\varphi & 0 \\ (a_n - a_s)sin\varphi cos\varphi & a_s cos^2\varphi + a_n sin^2\varphi & 0 \\ 0 & 0 & a_z \end{bmatrix} \tag{4.23}$$

The inertial resistance tensor ***B*** has the same form as ***A***. In the axial ***(z)*** as well as in the direction normal to the bristles ***(n)***, the flow experiences the full-drag, whereas the drag is expected to be much lower in the direction parallel to the bristles ***(s)***. There are six resistance coefficients $\boldsymbol{a_n, a_s, a_z, b_n, b_s}$ and $\boldsymbol{b_z}$ to be defined. It is assumed that $\boldsymbol{a_n = a_z}$, $\boldsymbol{b_n = b_z}$ and that all coefficients are uniform through a bristle pack and do not vary with pressure difference across the seal. The influence of the parameters on results can be summarized like:

- Mass-flow rate is controlled by the axial resistance $\boldsymbol{a_z}$ and $\boldsymbol{b_z}$,
- Backing ring pressure depends on mainly the level of the anisotropy.

More information about the experimental investigations of the resistance coefficients of anisotropic porous media can be found in Ergun [4].

The brush is modeled as a porous region with an anisotropic, nonlinear resistance law in present simulations. **Table 4.1** gives the parameters which are used. They are taken from Chew et al. and Chen et al. They have calibrated the porous medium approach against the measurement results of Bayley and Long.

	$\alpha_n = a_z\ [m^{-2}]$	$\alpha_s = \alpha_n/60\ [m^{-2}]$	$b_n = b_z\ [m^{-1}]$	$b_s\ [m^{-1}]$
low resistance	5,317 x 10^{11}	8,862 x 10^{9}	1,998 x 10^{6}	0
high resistance	7,440 x 10^{11}	12,400 x 10^{9}	2,800 x 10^{6}	0

Table 4.1 Resistance coefficients in the principal axes used for the simulation

5 Numerical Simulation

The scope of this work is using of commonly available CFD software for brush seal simulations. It is tried to reach to efficient brush seal CFD modeling by using a porous medium approach. Firstly, the experimental data from Bayley and Long are captured, such as mass-flow rate, pressure distribution on backing wall and rotor surface. After that the next simulations are applied for with compressible flow characteristic and clearance effect between rotor and bristle tips.

The software which is chosen for this purpose is ANSYS FLUENT 12.1. FLUENT is a flow-modeling tool with Finite Volume Method based solver. "Finite volume" refers to the small volume surrounding each node point on a mesh. Mesh is generated by GAMBIT.

The hardware used was Intel Core Duo Processor T2300 1.66 GHz processor and 2GB RAM.

5.1 Brush Seal Configuration

In this topic, it is given which geometry is used, how it is meshed, the properties of mesh and how it is approached to the problem.

The mesh is created in GAMBIT to simulate the brush seal. The Model which is used and simulated, are constructed based on Chew et al. [8] and Bayley and Long [1]. The geometrical Model is shown with detailed dimensions in **Fig: 5.1.**

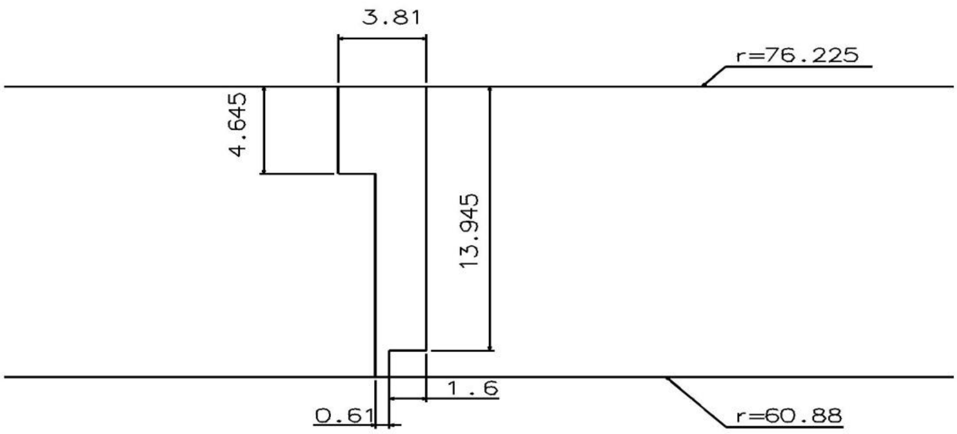

Fig. 5.1 Scheme of the brush seal, dimensions are in mm.

The mesh is generated in GAMBIT based on dimensions which are given by Bayley and Long. But for the model with clearance, there are also four different meshes. Their geometrical properties and mesh explanation and the model with full brush are given in the next parts.

In **Figure 5.2** mesh of brush seal is given.

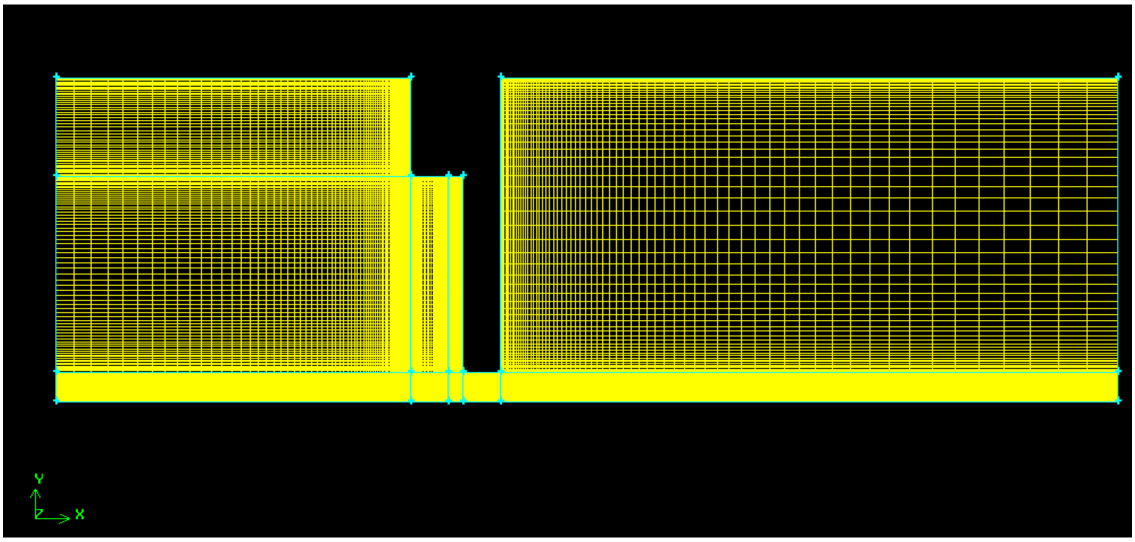

Fig. 5.2 Model of brush seal system. It was created in GAMBIT

If it is looked at the mesh structure, mesh is denser in the brush seal area and near the walls. The fence height region (the interference between the backing plate and the rotor surface) was meshed also denser. The mesh density should be more detailed in these regions, because the flow behavior is very complex here and for the exact solution, the mesh has an important role. If the turbulence occurs at flow, better solutions can be got by good quality mesh. In **Figure 5.3** can be seen the density of mesh at brush seal are.

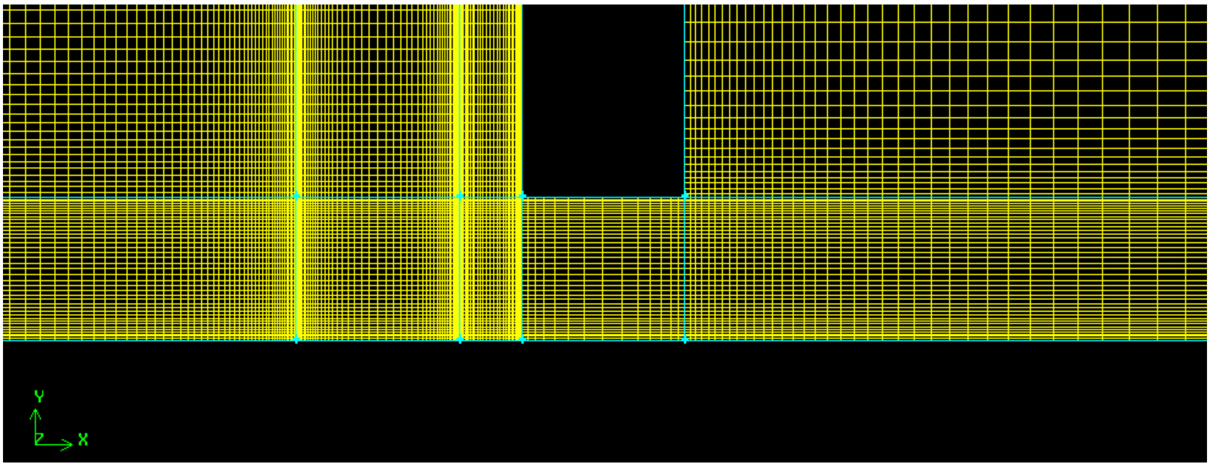

Fig. 5.3 Brush seal area, more detailed

For the models with clearance, the mesh is denser generated at the brush seal area and also between the brush tips and rotor. Because, the flow behavior is very complex between tips and rotor surface. Therefore, at the simulations, it is difficult to get exact and correct results without good mesh. In **Figure 5.4**, it can be seen an example for mesh density.

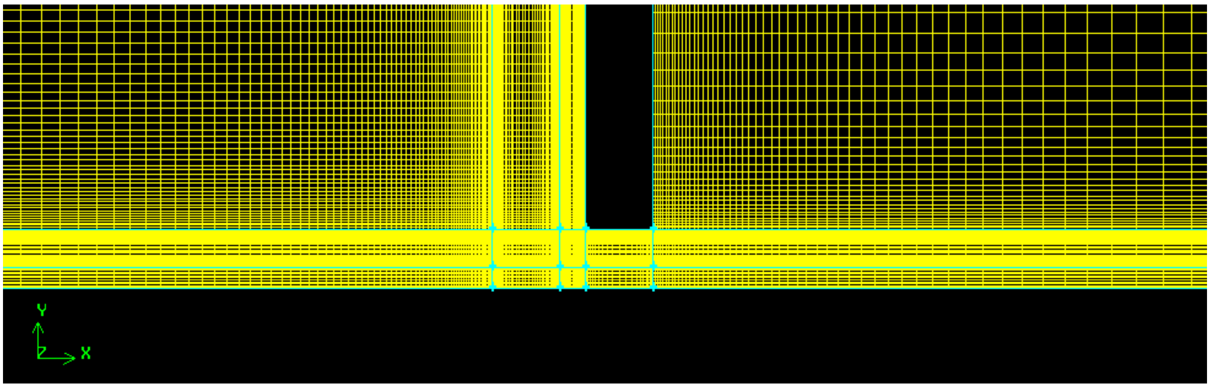

Fig. 5.4 Mesh figure for clearance with 0,27mm

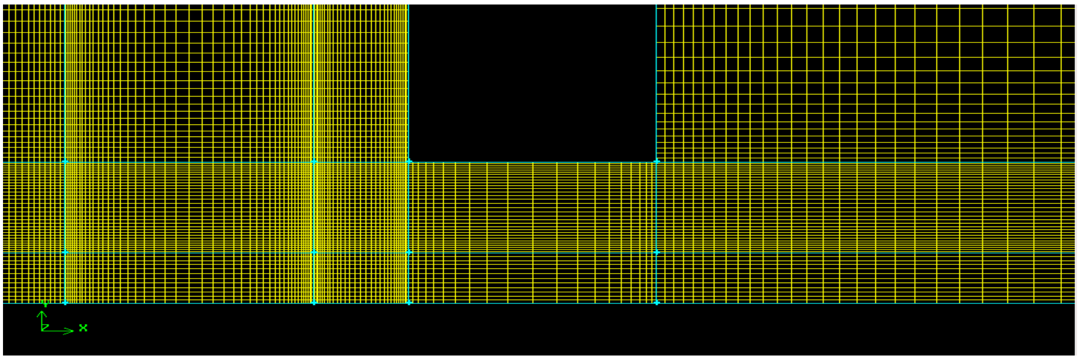

Fig. 5.5 Mesh figure for clearance with 0.27mm, more detailed

Near the walls, the mesh structure is also important, because after the simulation, the wall function should be for the standard for wall function $30<y^+<100$ or for enhanced wall function $y^+ \approx 1$. (It can be also accepted $y^+<10$) [28].

On the other hand, if the model has a denser mesh, it gives some problems. These problems are convergence occurring or convergence time during the simulation. There are some parameters that they affect the mesh quality and convergence. One of them is Aspect Ratio. It should be smaller than 10.

For ex. at the beginning, in incompressible simulations, which velocity inlet boundary condition is used, aspect ratio was so high. Because of this, the simulation couldn't get convergence, or if it got

$R_p = \frac{p_u}{p_d}$

convergence, it was with high iteration numbers like over 10000. After reducing the aspect ratio smaller than 10, simulations got convergence nearly with 900 iterations.

Before starting the simulation, it can be checked mesh quality. It gives opportunity to avoid from time waste and incorrect simulation results. There are two ways to do it. It can be checked in GAMBIT or in FLUENT. Here is explained how it is done in FLUENT. After reading the mesh file in FLUENT, first step should be scaling of model and then checking model. And if there is a problem with mesh, FLUENT gives a warning. With it error can be seen and it can be fixed in FLUENT or in GAMBIT. For more information about it, see FLUENT, GAMBIT help files and tutorials [30, 31].

5.2 Description of Simulation

In this work, four different simulations are applied. Brush seal is modeled with and without clearance for compressible and incompressible flows. Thus it is tried to find out the effect of radial clearance and compressibility. The aim of this simulation is to compare the results with existing one. The reference values are taken from Bayley and Long [1]. After capturing the results from the literature, secondly, in part 2, it is tried to find the effect of compressible flow in simulations. It is compared with the first simulation.

At the last part, in results part-clearance it is examined the effect of clearance between the bristle tips and rotor surface.

At the end of the all simulations, the results are taken:

- To compare of mass flow versus pressure ratio,
- Radial pressure distribution at the backing wall,
- Axial pressure distribution at the rotor surface,
- And the behavior at the brush area.

In simulations, porous medium approach is used to simulate airflow through a bristle pack. The bristles are represented by an anisotropic permeability tensor. For all simulations, the $k-\epsilon$ model is used for turbulent flow.

The ideal gas law applied for the compressible air flow. For the incompressible flows, the velocity values are taken from the mass flow rates. Downstream boundary is always kept at atmospheric pressure. The air at inlet temperature set constant at 293,15 K. The pressure ratios

$$R_p = \frac{p_u}{p_d} \qquad (5.1)$$

where $\boldsymbol{p_u}$ upstream pressure and $\boldsymbol{p_d}$ downstream pressure is, are varied from ***1,5*** to ***4***.

5.3 Description of Input of Simulation and Giving of Boundary Conditions

Firstly “Import the mesh file.”

“File → Read → Mesh / Case& Data”
Here, the mesh file which is generated in GAMBIT is imported.

- Solver adjustment in General Task Page
  “Define→ Problem Setup→ General”
  After the mesh file is imported, the basic solver setting is here given.

Type	Pressure-Based Solver
Velocity Formulation	Absolute
Time	Steady
2D Space	Axisymmetric Swirl

Table 5.1 Solver-Settings

Table 5.1 shows the basic solver settings for 2D Simulations with the Pressure-Based Solver Type. For type, Pressure-Based Navier Stokes Solution algorithm is enabled. Velocity formulation is switched to absolute Velocity. With Steady option it is specified that a Steady flow is being solved.
For simulations, axisymmetric Swirl Option is chosen. It is important to get circumferential component. This option specifies that the swirl component (circumferential component) of velocity is to be included in axisymmetric model.

- The scale of Mesh
  “Define→ General→ Mesh→ Scale”
  Mesh option controls geometrical properties like mesh quality and model dimensions. After importing mesh file from GAMBIT to FLUENT, it should be controlled the dimensions of model. And the scale mesh option allows converting the mesh to various units of measurements. It can be also applied custom scale factors to the individual coordinate of the mesh.

  In the Mesh-dialog box, it can be also controlled how good mesh is.

  Mesh→ Check
  If there is a problem about mesh, there is a warning about it.
  Mesh→ Report Quality

It can be become the information about mesh quality parameters such as maximum cell squish, maximum aspect ratio.

- Mesh – Reorder
  After scaling mesh, it is option to reorder mesh

  Mesh→ Reorder→ Domain
  Mesh→ Reorder→ Zones

- Selection of Calculation Model
  "Define→ Models→ Viscous"
  k-ε, realizable, standard wall function is used.

  "Define→ Models→ Energy"
  It is up to solution if it is compressible or incompressible. It is used energy on for the compressible simulations and energy off for incompressible simulations.

- Materials properties
  "Define→ Materials→ Fluid"

In simulations, two different flow types are applied, compressible and incompressible. For solutions energy equations and different fluid types are used by ANSYS. As a fluid, air is taken for present analyses.

To input its properties, under materials→ Create/ Edit Materials section is used.

For the incompressible flow two different approaches are used. First simulation is modeled with velocity inlet boundary condition. For the air option, under the material properties the following values are applied.

$$\rho = 1{,}21\, kg/m^3 \text{ and } T = 20°C\ .$$

Another simulation is modeled with pressure inlet boundary condition. But here it should have been careful, because by increasing inlet pressure, the density should increase too. In **Eq. 5.2** can be seen that there is a direct ratio between $\boldsymbol{\rho}$ and $\boldsymbol{p}$**.**

$$\rho = \frac{p}{RT} \tag{5.2}$$

where T and R constant are. Therefore **Table 5.2** is prepared for the $R = 1,5\ to\ 4$ to input for material properties.

p_1 [bar]	ρ [kg/m³]	c_P [J/kgK]	λ [W/mK]	η [Pa s]
1,5	1,782	1007,237	0,02589	$1,8212*10^{-5}$
2,0	2.376	1008,075	0,02591	$1,8219*10^{-5}$
2,5	2,970	1008,913	0,02592	$1,8226*10^{-5}$
3,0	3,564	1009,750	0,02594	$1,8233*10^{-5}$
3,5	4,158	1010,588	0,02595	$1,8240*10^{-5}$
4,0	4,752	1011,425	0,02597	$1,8247*10^{-5}$

Table 5.2 The air properties for different inlet pressure at 293,15 K

In **Table 5.2**, the whole air data such as ρ, c_P , λ, η by 20°C temperature and was calculated with interpolation.
In the simulation of compressible flow, air is selected as ideal gas.

- Definition of Cell Zone Conditions
  “Define→ Cell Zone Conditions→ Zone”

In this section, brush zone properties are given. Brush is selected as a fluid in FLUENT. Before giving the zone properties by ANSYS, these zones must be defined in GAMBIT. In FLUENT, just the data of properties are applied for each zone. Air is selected for a fluid type. The properties of air are defined under material properties.

For the brush zone, it is selected porous zone and the data from porous medium is entered. **Table 5.3** gives us the data of porous medium. The values are taken from Chew at al.

	$\alpha_n = a_z\,[m^{-2}]$	$\alpha_s = \alpha_n/60\,[m^{-2}]$	$b_n = b_z\,[m^{-1}]$	$b_s\,[m^{-1}]$
low resistance	$5,317*10^{11}$	$8,862*10^{9}$	$1,998*10^{6}$	0
high resistance	$7,440*10^{11}$	$12,400*10^{9}$	$2,800*10^{6}$	0

Table 5.3 Resistance coefficients in the principal axes used for the simulation

And the porosity is as 0,3 selected.

- Specifying operating conditions

  It is defined here the operating pressure and the gravity. FLUENT works with the Gauge pressure. It means, what is entered, is given over the “operating pressure”. FLUENT takes the operating pressure 101325 Pa. **Figure 5.6** explains the pressure logic in FLUENT.

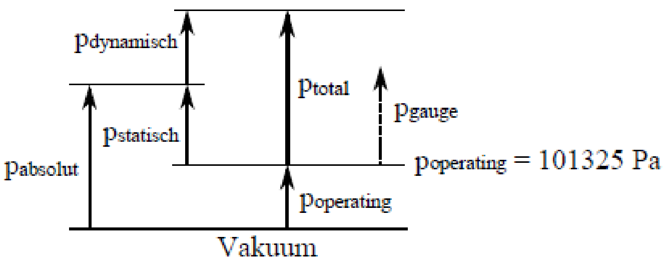

Fig. 5.6 Pressure explanation [12]

- Boundary Conditions

  The first boundary conditions are defined to model in GAMBIT. They are reference zones for FLUENT simulations. In FLUENT, the boundary conditions are applied again.

  <u>Inlet Conditions:</u>

  For the incompressible Flow

  “Define→ Boundary Conditions→ Zone→ Velocity Inlet”

  As boundary condition for entrance velocity inlet is applied.

  For the compressible Flow

  “Define→ Boundary Conditions→Zone→ Pressure inlet”

  In these simulations, as boundary condition, pressure inlet is selected for the entrance and the pressure ratio must be defined to the ANSYS. It is taken ***1,5*** to ***4***.

  <u>Outlet Conditions:</u>

  For the compressible and incompressible Flow, outlet conditions will be same.

  “Define→ Boundary Conditions→ Zone→ Pressure Outlet”

  The outlet Pressure is stabilized with 0 Pa, it means it is at atmosphere pressure.

Wall Conditions:

The simulations without swirl

"Define→Boundary Conditions→ Zone→ Wall"

Rotor and Walls were selected as wall and

Wall Motion→ Stationary Wall

Shear Conditions→ No Slip

For compressible flow analyses, constant temperature with 300K and adiabatic wall is chosen.

- Solution Conditions

Solve→ Solution methods→ Pressure→ Velocity Coupling

For Incompressible Flow→ SIMPLE

For Compressible Flow→ COUPLE is used.

With coupled option, ANSYS gives better result for compressible flows.

Solve→ Solution Methods→ Spatial Discretization

For the incompressible Flow, **Table 5.4** shows the data, which are applied.

Gradient	Least squares Cell Based
Pressure	Standard
Momentum	Second-Order-Upwind
Swirl Velocity	Second-Order-Upwind
Energy	Second-Order-Upwind

Table 5.4 Discretization at incompressible flow

For the compressible Flow, **Table 5.5** shows the data for the simulation.

Gradient	Least squares Cell Based
Pressure	Standard
Density	First-Order Upwind
Momentum	Second-Order-Upwind
Swirl Velocity	Second-Order-Upwind
Energy	Second-Order-Upwind

Table 5.5 Discretization at compressible flow

- Solutions Controls

  It is kept here the default conditions in FLUENT as seen in **Fig. 5.7.**

Pressure	0.3
Density	1
Body Forces	1
Momentum	0.7
Swirl Velocity	0.9

Fig. 5.7 Solution controls sector in FLUENT

- Monitors

“Solve→Monitors→Residuals, Static and Force Monitors”

It is changed here the convergence absolute critters to $1*10^{-5}$. While solution is running, if the iterations reached this level, the convergence is become.

“Solve→ Monitors→ Surface Monitors”

This option gives an opportunity to point out, what is wanted to look at during the simulation. For ex. In present simulations, scaled residuals and mass-flow-rate at inlet are defined. Thus, during simulation, these data can be followed on screen. Mass-flow-rate can be seen at inlet how it changes with time.

Name → Mass Flow
Report Type → Mass Flow Rate
Surface → Entrance
Options →Print to Console
Plot to 2. Window

- Solution Initialization

  “Solve→Solution Initialization”
  Before starting the calculation, it should be initialized.

  Compute from→ All Zones
  Initialize
  In this section, there are also other options like reset and patch. Some simulation data which are applied before, can be changed here to get a better solution. For more information, see in FLUENT Help Files [30].

- Running the calculation

  “Solve→ Run Calculation”
  In this Section, before beginning the calculation, it should be given firstly the number of iterations. On the other hand it can be also arranged the reporting interval and profile update interval. After doing these arrangements, model is checked and if there is a problem, ANSYS gives a warning for it. This warning comprises following headings.

  Mesh/Model/ Bounders and Cell Zones / Material/ Solver

  If there is warning about simulations, under the related tab (for ex. Mesh or Material or Solver) there is a explanation for it. This explanation can be seen with clicking “**?**” figure. Although ANSYS gives a warning, it doesn’t mean that, model is 100% wrong. FLUENT gives a tip that there are alternative solution approaches or development possibilities at model to get better solutions.

  If everything is ok, then it can be started to calculation from “Calculate”

5.4 Results

At the present work, the brush seal is modeled in GAMBIT and simulated in FLUENT. The results are compared firstly with the data from the literature and then the research is extended.

At the beginning, it is examined that mass flow rate and bristle pack pressure distribution. The compared data are taken from Bayley and Long. The first simulation was incompressible and without rotational velocity. The results show that the data are the same with the experimental data from literature [1].

After that, the same simulation is performed as a compressible flow and the effect of the compressibility is examined.

At the end of this work, the clearance effect is observed. There are some literature researches [11, 13 and 14] and from these literatures, it can be seen and predicted the flow behavior and clearance effect on the brush seals. In simulations, it is tried to come close to these behaviors and data.

All these simulation results are explained and discussed partly at the next section. For all simulations, the boundary conditions and the theoretical information are given at the previous section **5.3**.

Furthermore, for comparing the results the non-dimensionalising for the all values is applied.

To obtain non-dimensional distance in ***x*** and ***y*** directions, one has to divide dimensional value by inlet height. Inlet height was chosen as a reference dimension. Inlet height is equal to 0, 015345 [m]. The information at dimensional distance into non dimensional was done such:

$$x^* = \frac{x}{h1} \qquad (5.3)$$

$$y^* = \frac{y}{h1} \qquad (5.4)$$

The way of obtaining pressure ratio is shown next. But it is written for dimensional values.

$$R_p = \frac{P_u}{P_d} = \frac{P_d + \bar{P}}{P_d} = 1 + \frac{\bar{P}}{P_d} \qquad (5.5)$$

For non dimensional quantities, the following equation is used

$$R_p = 1 + \frac{\bar{P}^* \rho v^2}{P_d} \qquad (5.6)$$

Where

$$\bar{P}^{*} = \frac{\bar{p}}{\rho v^{2}} \qquad (5.7)$$

In conclusion, the **Eq. 5.5** is used to obtain pressure ratio.

$$R_{p} = 1 + \frac{\bar{P}^{*} \rho v^{2}}{1bar} \qquad (5.8)$$

For the graphical results, it is used the dimensionless pressure $\boldsymbol{p_{nd}}$. It is calculated by,

$$p_{nd} = \frac{p_{a} - p_{d}}{p_{u} - p_{d}} \qquad (5.9)$$

In the radial pressure distribution ***Y*** is used radial coordinating. This coordinate was calculated using following equation.

$$Y = \frac{y}{h_{bf}} \qquad (5.10)$$

It is a non-dimensional value. Bristle free height is a distance of bristle from tip to the bottom of front plate. It can be also expressed that part of bristle which is exposed to the stream without any protection.

The fence height, in normalized radial coordinate, equals to:

$$h_{fh} = 0{,}0014m.$$

The next two parts **5.4.1** and **5.4.2** are taken together to compare. At the first part, the flow is taken incompressible, on the contrary at the second part compressible. At below firstly, there is pre-information about these two simulations, and then the detailed information is given. At the end, it is showed the comparison of these two simulations with the flow fields and flow behavior.

5.4.1 For the Incompressible Flow

The aim of simulation is to compare the results with existing ones, Bayley and Long [1]. The geometrical data are taken from Bayley and Long. To compare the results, the most common and significant ratio, mass flow versus pressure ratio is used. After the simulation, the results will be compared with the literature and model will be validated, thus it can be gone on to the other simulations.

For the first simulation, velocity inlet boundary condition is used. Reference velocities are computed from each mass flow rates which are given like:

- $\dot{m} = 0{,}005\ kg/s$
- $\dot{m} = 0{,}008\ kg/s$
- $\dot{m} = 0{,}010\ kg/s$
- $\dot{m} = 0{,}015\ kg/s$.

For the velocity values,

$$\dot{m} = \rho v A \tag{5.11}$$

is used in each simulations where $\rho = 1{,}21\ kg/m^3$ is chosen constant as average value.

It can be also used here mass flow rate as inlet BC. The velocity distribution is constant in the radial direction.

It is here also important that the controlling of our turbulence. Because the $k - \epsilon$ turbulance model is used.

For the controlling, ***Re number*** can be calculated.

$$Re = \frac{vh}{v} \tag{5.12}$$

At the inlet, ***Re number*** is small approximately 1046 but at the brush seal area it reached the high numbers. Therefore the choice of turbulence model is true.

In this simulation, the rotor is accepted as stationary and the flow is incompressible. At the outlet boundary condition is accepted atmospheric Pressure 101325 Pa.

5.4.2 For the Compressible Flow

In this simulation, compressible-flow is searched. The Model geometry is taken from the research of Bayley and Long like at the first simulation. It is investigated that, how mass-flow-rate changes with the pressure ratio.

Actually it isn't expected that, there is a significant change in this solution. Because for the compressible flow, the mach-number is important. If $\boldsymbol{Ma} > 0{,}3$ is, there is a significant changing at density values. Mach number is defined with **Eq. 5.13**.

$$Ma = \frac{v}{a} \tag{5.13}$$

The density effects are important. With this simulation for the $1.5 < \boldsymbol{Rp} < 4$, it will seen the $\boldsymbol{v}$ values and then it can be said something about $\boldsymbol{Ma}$ number and after that it will be compared with the incompressible flow under the same conditions. In **Chapter 5.6,** $\boldsymbol{Ma}$ values can be seen.

For the compressible flow, ideal gas assumption is taken.

In this simulation, $k - \epsilon$ turbulence model is used, the rotor is accepted stationary and adiabatic, at the outlet boundary condition, air is at atmospheric Pressure 101325 Pa.

5.5 Results Part 1 – Incompressible Flow

5.5.1 Mass Flow Rate

The mass flow rate is a quantity which characterizes leakage of the brush seal which is the most important parameter of a turbomachinery seal. **Figure 5.8** shows the computed mass flow rates versus the pressure ratio. The values of Bayley and Long were extracted from Chew et al. [8]. They are the experimental data.

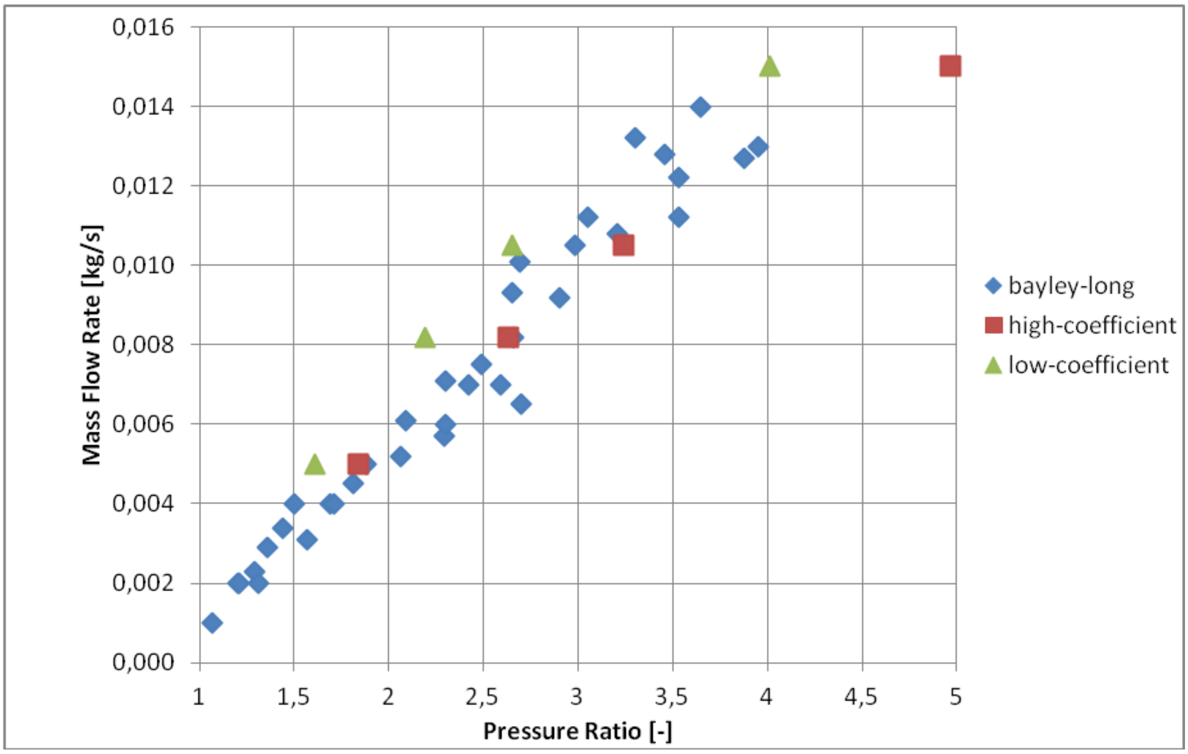

Fig. 5.8 Comparison of computed and measured mass flow rates versus pressure ratio

Figure 5.8 shows that the present CFD calculations match the experimental values of Bayley and Long [1]. If it is looked at the data, the values from simulations of high-resistance-coefficient are more accurate than low-resistance-coefficient. With the increase of pressure ratio, the mass flow rate also rises, and this is expectable. High-resistance- coefficient represents the brush seal with tighter bristle pack. By increasing pressure load the tightening occurs. It means normally that the permeability of the coefficients is not constant during the experiment however; this simulation is based on constant permeability of the coefficients. Nevertheless, considering the range of pressure ratio, there is a good leakage agreement with the experiments.

Furthermore, we know from the equations in **Chapter 4** the mass flow rate is mainly influenced by the axial coefficients a_z and b_z. The influence of the resistance coefficients can be shown from the different leakage behaviors.

5.5.2 Axial Pressure Distribution

The second parameter to compare the results of CFD with literature is the axial pressure distribution on rotor surface. The results of the simulations are compared with the experimental data by Bayley and Long. There is a high axial pressure load which is subject to the brush seal. Pressure drops down significantly from upstream to downstream side through the brush seal. **Figure 5.9** shows this pressure drop. The dimensionless pressure p_{nd} is plotted versus axial coordinate z. The obtaining of the p_{nd} is already given at the previous section.

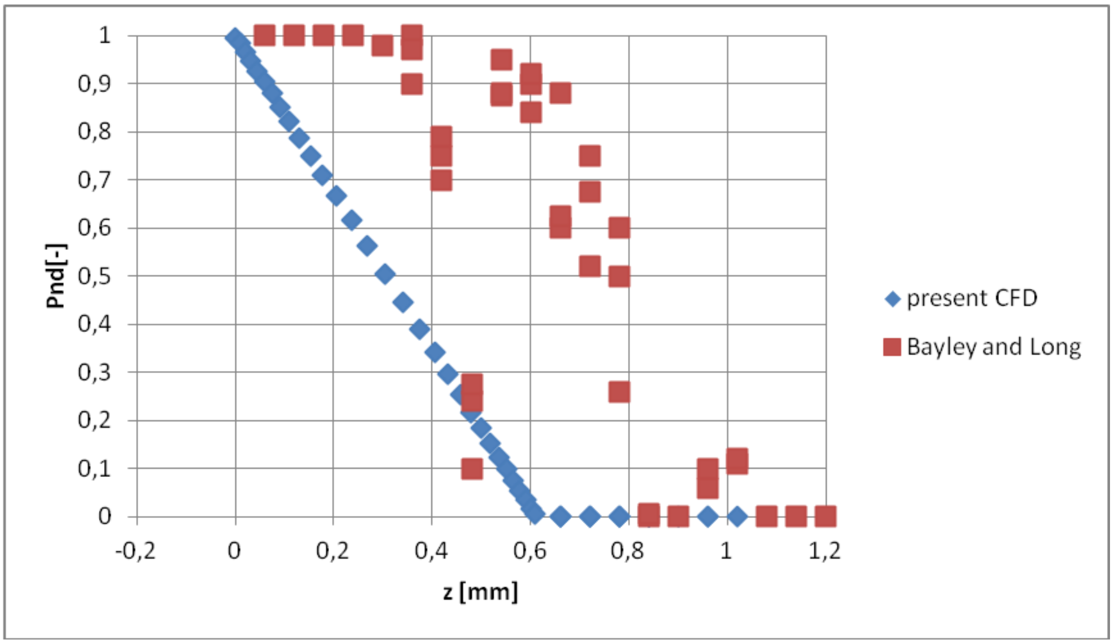

Fig. 5.9 Comparison of axial pressure distribution on rotor surface

In **Figure 5.9**, bristle pack thickness is between z 0,0 to 0,6mm. The local coordinate starts at z=0 at the upstream plane of the brush. From the **Fig. 5.9**, it can be seen that the pressure drop occurs through the bristle, and it is almost linear. The experimental values from Bayley and Long show no clear trend. The reason for it is high scatter of the data. This scatter is observed by Bayley and Long, which is a result of circumferential variations in the axial deflections of the brush seal. On the other hand, Braun et al. (1990) as independent from Bayley and Long confirms this almost linear pressure gradient.

Furthermore, as can be seen from the figure, there is an offset in the axial direction of about 0.4mm between measured and computed pressure distribution. This is because of the bending of the bristles in axial direction as a result of pressure difference. In industrial applications, bristles in fence height region are free to bend in axial direction depending on the balance of aerodynamic, elastic, and frictional forces.

5.5.3 Radial Pressure Distribution

In **Figure 5.10** is shown the distribution of the non-dimensional pressure p_{nd} versus the non-dimensional distance ***Y***. Y is the coordinate in radial direction at the interface between brush and backing plate. The origin is located at the rotor surface and Y=1 indicates the corner between the bristle pack and the front plate. Non-dimensionality is explained in the previous section.

The simulation results are compared with the experimental data of Bayley and Long for highest and lowest pressure ratios. In the CFD simulation, it is observed that the pressure drop occurs in the region of Y < 0.3 however, the experimental data indicates a significant drop from Y=0.4. The pressure on the backing plate for the upper region is almost constant and nearly equal to upstream pressure. The pressure drop occurs in the region of backing plate, and downstream pressure is gained here. This pressure distribution indicates a pressure gradient from the upper region to fence height area directing the flow radially inward. Actually, in the real life, the bristle pack behaves a little differently because of the blow down effect. The pressure causes bristles to move towards the rotor surface.

In the next section, the flow behavior will be shown, and in these sections it is clearer to understand the pressure distribution among the bristle pack.

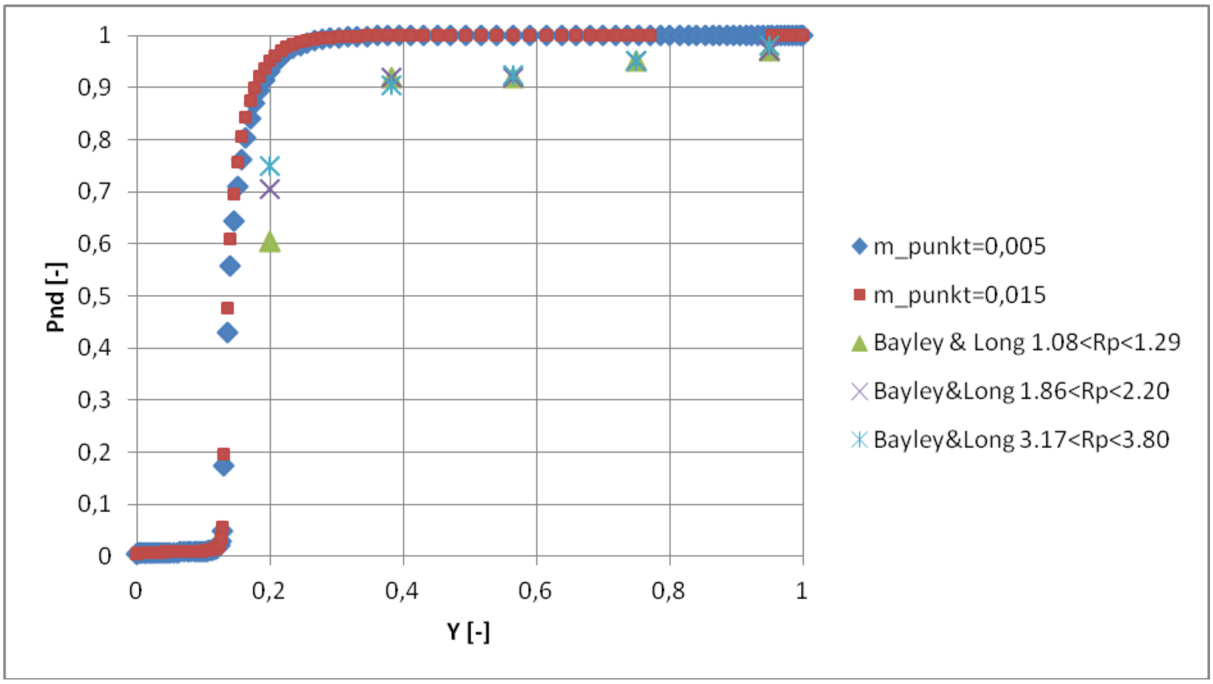

Fig. 5.10 Comparison of radial pressure distribution on backing plate

5.6 Results Part 2 – Compressible Flow

5.6.1 Mass Flow Rate

As the results of part 1 are stated in the previous section, it is explained that the mass flow rate is a quantity which characterizes the leakage of the brush seal, the most important parameter of a turbomachinery seal. In this simulation, the effect of the compressible flow is searched and examined. The results are compared with the experimental data of Bayley and Long, and also with the incompressible flow data shown in the first section. **Figure 5.11** demonstrates the mass flow rate versus pressure ratio.

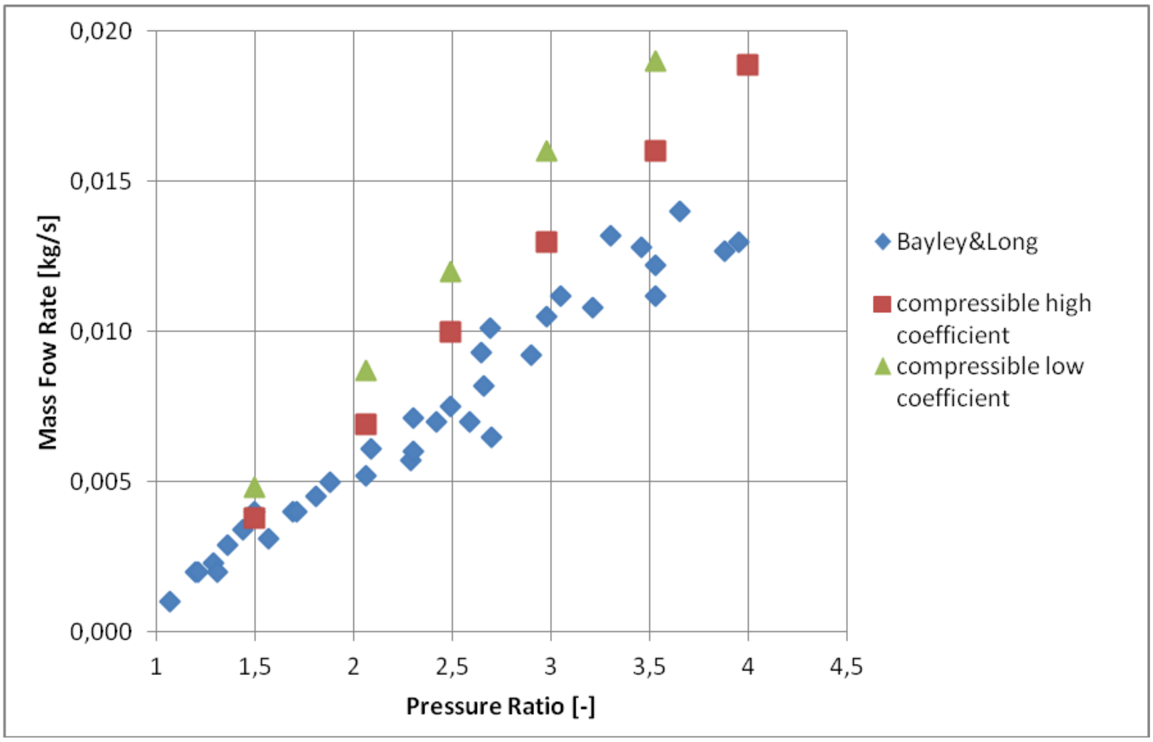

Fig. 5.11 Comparison of computed and measured mass flow rates versus pressure ratio

As seen from the **Fig. 5.11**, the results are a little overestimated with the experimental and incompressible flow data. The mass flow rate increases with the pressure ratio. With the high resistance coefficients, the simulation results are more accurate than the low resistance coefficients. The different leakage behaviour between the high and low resistance coefficients can be seen obviously.

On the other hand, the **Fig. 5.11** indicates that the resistance increases with increasing pressure ratio. This is due to the fact that the packing density of the bristle pack increases with increasing pressure ratio [2].

If the results of the incompressible flow simulations are examined, it is said that the results of incompressible flow gives more accurate solutions. It can be questioned whether the compressible simulation for the brush sealing is needed. If it is looked at the velocity distribution at the whole model, it is seen that max velocity is 65m/s if the mach number is considered.

$$Ma = \frac{v}{a} \ll 1 \qquad (5.14)$$

Therefore, if the mach number from the equation 5.13 for this simulation is calculated,

$$Ma = \frac{65}{340} = 0{,}19 \qquad (5.15)$$

Where $\boldsymbol{a} = 340m/s\ for\ 288.15K\ and\ 101325Pa$.

It can be seen that it is at the region of **Ma<0.3** , it means that it is in incompressible region. Mach number values can also be taken directly from the simulation results. The FLUENT allows to take the mach number for different pressure ratios.

In conclusion, it can be said that at this simulation with these values, the compressible flow has no significant good effect on the results. On the other hand, the long calculation time with the compressible flow can be considered. Finally, it can be seen that the incompressible flow is convenient for these simulations if the mass flow rate parameter is taken into consideration. Since they are well matched with the experimental data in a better way than compressible flow analyses, it takes less time to calculate like compressible flow simulation.

5.6.2 Axial Pressure Distribution

The second parameter to compare the results of CFD with literature is the axial pressure distribution on rotor surface. The results of the simulations are here compared with the experimental data by Bayley and Long and with the simulation of incompressible flow. **Figure 5.12** shows the axial pressure distribution on the rotor surface. The dimensionless pressure p_{nd} is plotted versus axial coordinate z. The obtaining of the p_{nd} is already given in the first section.

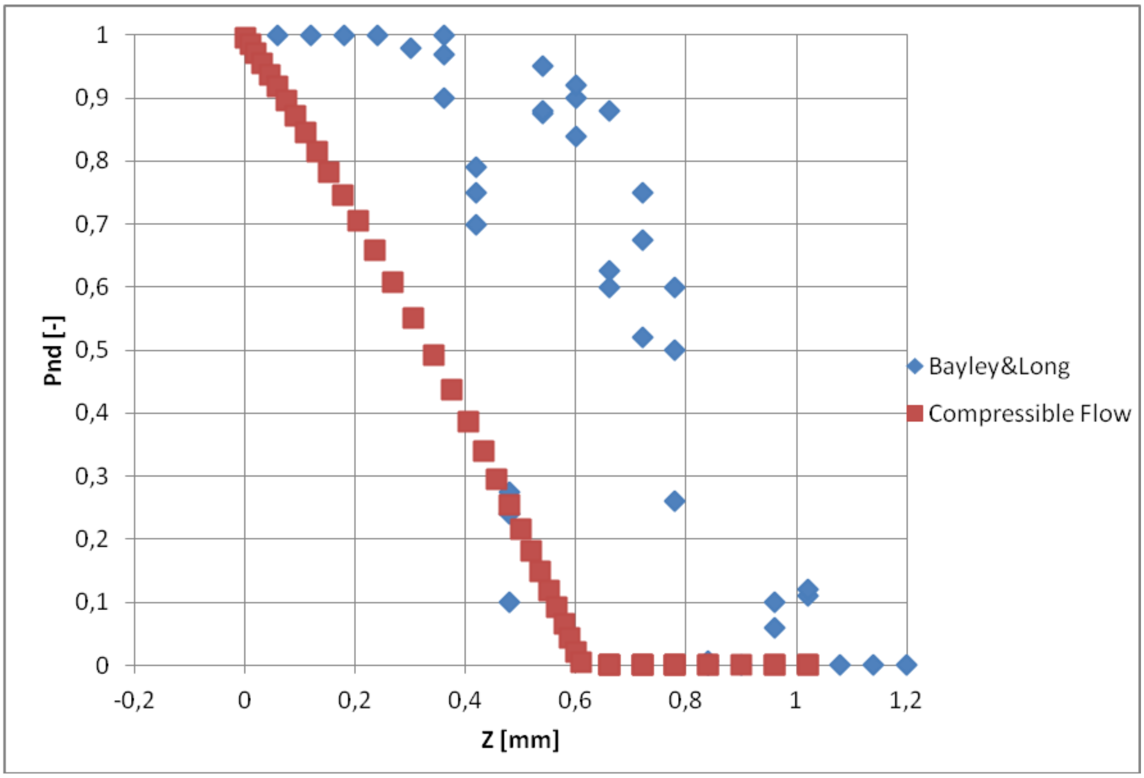

Fig. 5.12 Comparison of axial pressure distribution on rotor surface

The pressure distribution is nearly the same with the incompressible flow. Through the brush seal, pressure drops down significantly from upstream to downstream side. From Fig. **5.12**, it can be seen that the pressure drop occurs through the bristle, and it is almost linear. The experimental values from Bayley and Long show no clear trend. The reasons are explained in detail in the incompressible flow section.

To summarize, it can be said that at the compressible flow simulation, the flow behaviour and the pressure distribution behave in a similar way to the incompressible flow, and it was expectable. The compressibility has no significant effect on the axial pressure distribution on the rotor surface.

5.6.3 Radial Pressure Distribution

In **Figure 5.13** the distribution of the non-dimensional pressure p_{nd} versus the non-dimensional distance Y is shown. p_{nd} and Y were explained previously.

The simulation results are compared with the experimental data of Bayley and Long for highest and lowest pressure ratios, and with the data from incompressible flow simulation. In the compressible and incompressible CFD simulation, it is observed that the pressure drop occurs in the region of Y < 0.3 however, the experimental data shows a significant drop from Y=0.4. The reasons for it and the flow behavior are not explained in detail because they are given in the incompressible flow simulation.

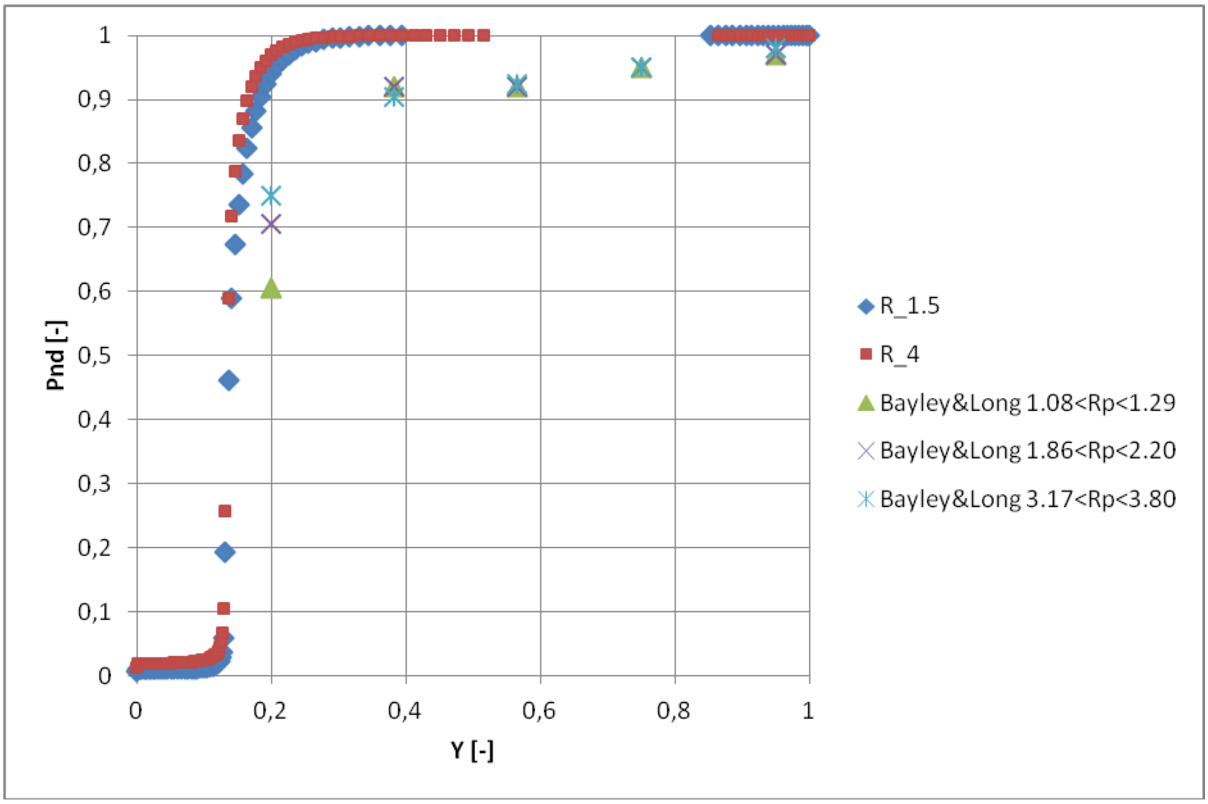

Fig. 5.13 Comparison of radial pressure distribution on backing plate in compressible flow

As seen from the **Fig. 5.10** and **5.13** there is no significant difference on the radial pressure distribution at the backing plate between the incompressible and compressible flow.

5.6.4 Flow Fields and Flow Behaviour

In this section the flow behaviour of the incompressible and compressible flow are given together and comparative.

Figure 5.14 and **5.15** show the pressure gradient at the fence region for two simulations: compressible and incompressible flow. It is visible that pressure drop occurs directly in the bristle pack at the fence height region. The gradient is very high on the small distance for two cases: compressible and incompressible flow.

As it can be seen from both of the figures, the pressure gradient is the same for two simulations as expected.

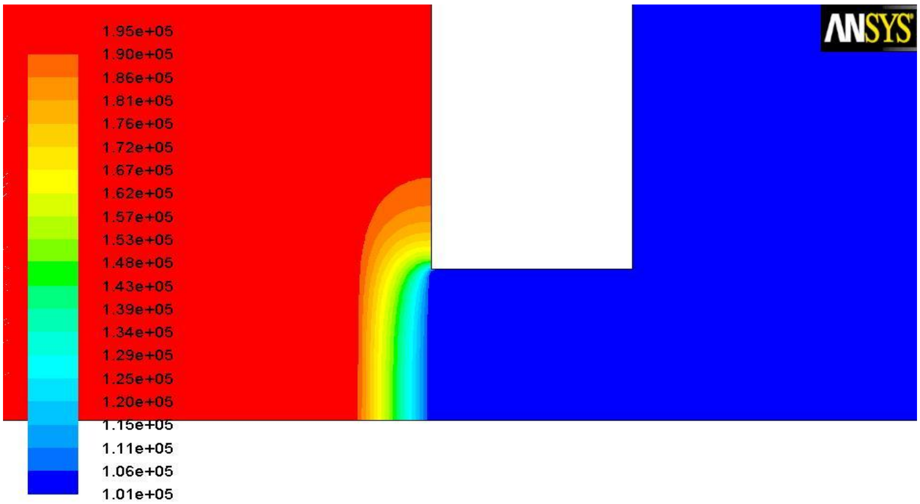

Fig. 5.14 Pressure gradient in fence height region, incompressible flow

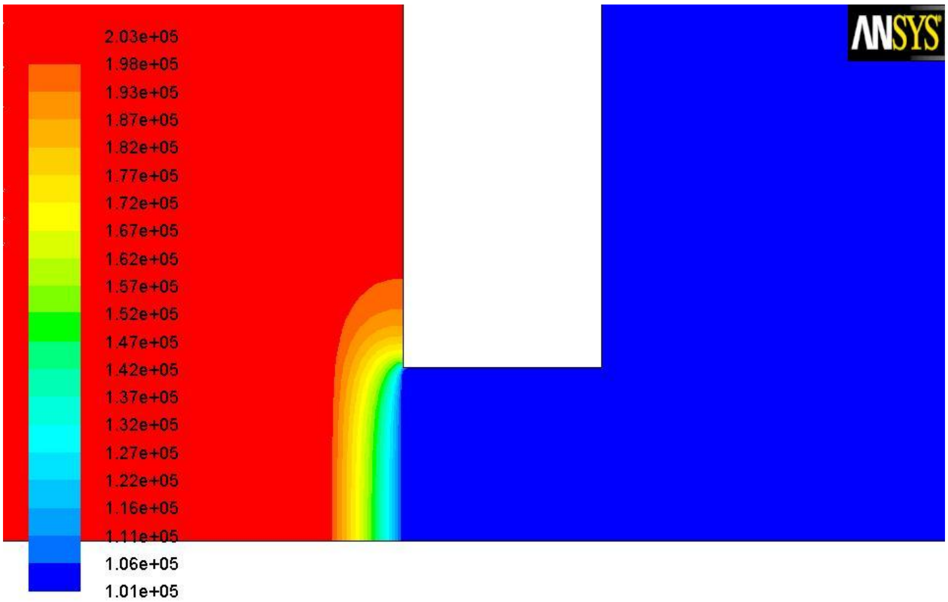

Fig. 5.15 Pressure gradient in fence height region, compressible flow

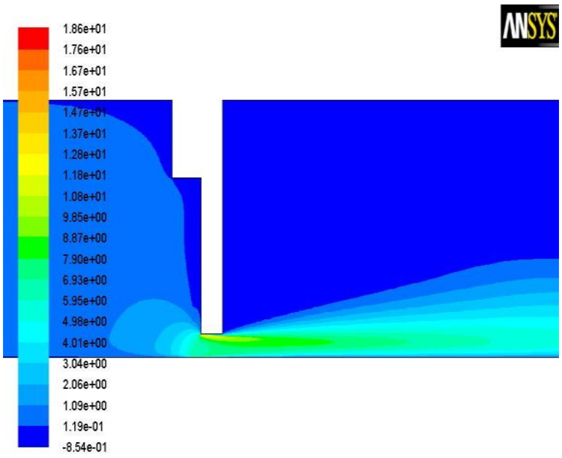

Fig. 5.16

Contour plot of axial velocity in incompressible flow

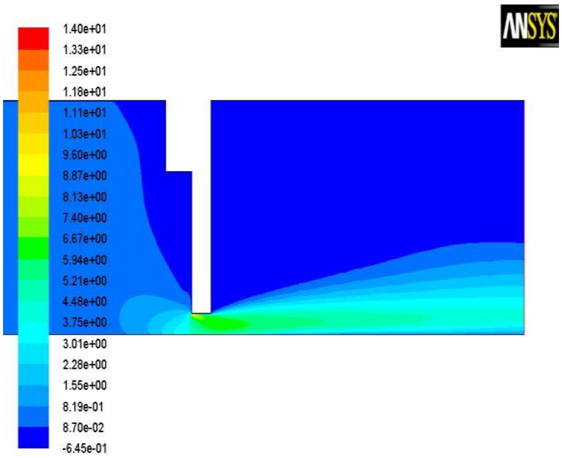

Fig. 5.17

Contour plot of axial velocity in compressible flow

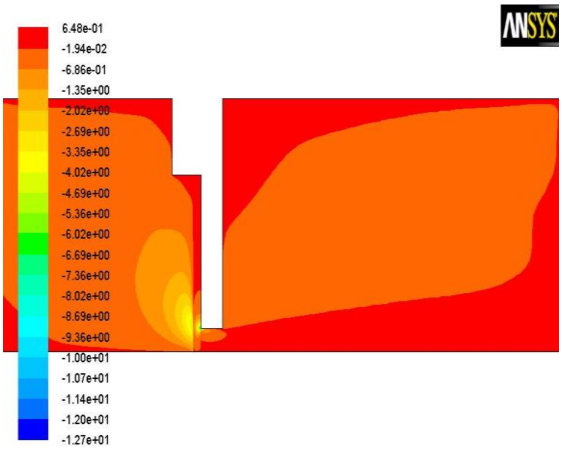

Fig. 5.18

Contour plot of radial velocity in incompressible flow

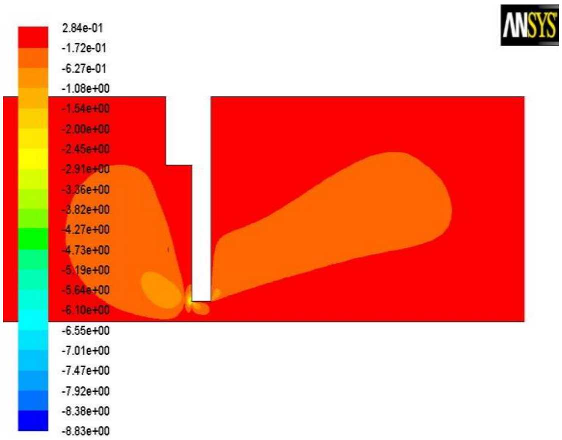

Fig. 5.19

Contour plot of radial velocity in compressible flow

Figure 5.16 to **5.19** give the contour plots of the axial and radial velocity for two simulations of compressible and incompressible flow. There is no significant difference between them. For more detail the figures of the velocity vector field for two simulations are given. Then, the results can be evaluated and compared more conveniently.

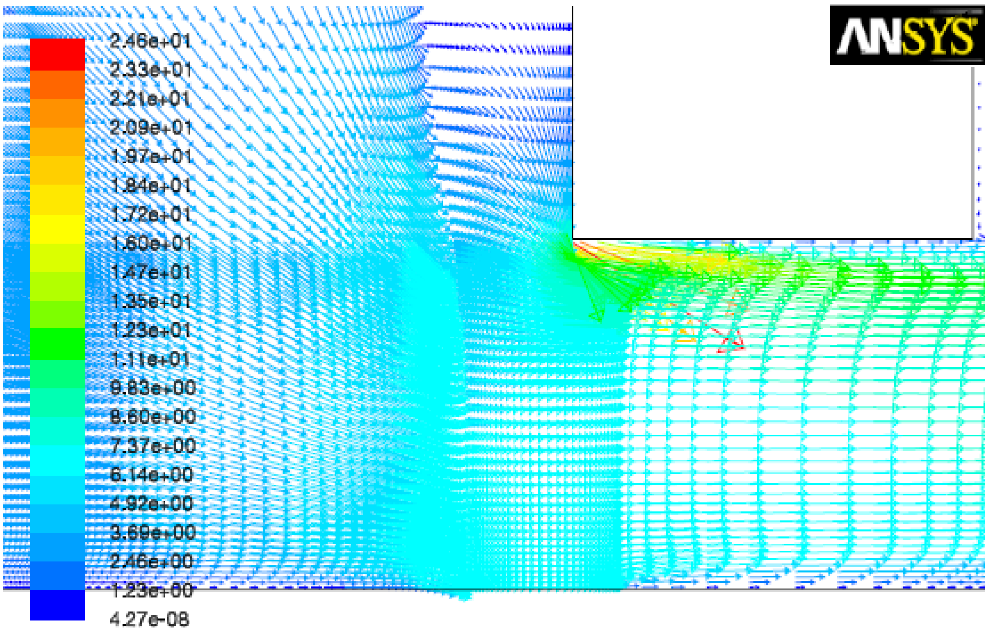

Fig. 5.20 Velocity vector field for incompressible flow

In **Figure 5.20** and **5.21**, the velocity vector field in the brush seal region is shown. As it can be seen from the figure, the flow follows the front part of the brush seal, and the velocity vectors move first at the edge radially to the brush. In another word, they move downwards, and then they try to pass the fence height region. Surely, the bristles block the flow there. The stream has a lower pressure after passing the bristle pack, and it tends to occur in the down-stream cavity.

Theoretically, the stream should significantly redirect its path when entering into the bristle pack at the higher regions of the seal. If the bristle pack region is examined more deeply, it can be said that, as expected, the stream should be parallel to the bristles in the bristle pack, and in the simulation, the flow enters into the bristle pack. It tends to flow radially, and near the backing plate it takes a form parallel to the bristles. Probably, it does not develop exactly at the entrance area in this CFD simulation, but the results are acceptable.

At the backing plate corner, the stream accumulates and enters into the cavity between backing plate and rotor cover surface. From **Fig 5.20** and **5.21**, it can be seen that, the velocity reaches its maximum value in both radial and axial directions. It is obvious from the velocity vectors from **Fig. 5.21.**

The downstream face of the bristle pack in fence height region is subject to relatively higher axial velocities. This velocity tends to pull the bristles from the last columns of the pack towards the downstream part of the fence height region. Bristles tend to flutter because of this process. Fluttering depends on the balance of forces. It was theoretically explained previously.

If more detail is given about the back side of the backing plate, it is required to state that there is a recirculation. It occurs because the channels diameter is narrowed by installing brush seal, and then the channels diameter is enlarged again. This recirculation is expectable. The brush seal, or the bristle pack itself has no significant influence on the process. However, this process can cause the stream recirculation under the backing plate. It can be explained that the flow accelerates with the effect of brush seal, and then the geometry enlarges at that time and causes this recirculation.

Finally, it is evaluated in this study that the velocity vectors for the compressible and incompressible flow together. As it can be seen from **Fig. 5.20** to **5.23,** it is obvious that the flow behaves in the same way in these two different cases. The numerical values are not given here because the aim is to understand the flow behaviour.

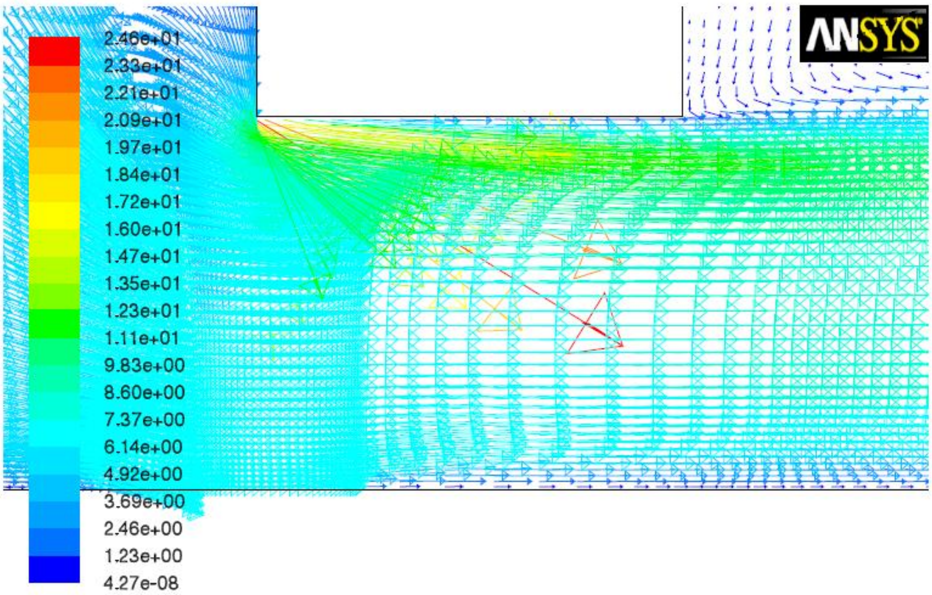

Fig. 5.21 Velocity vector field more detailed for incompressible flow

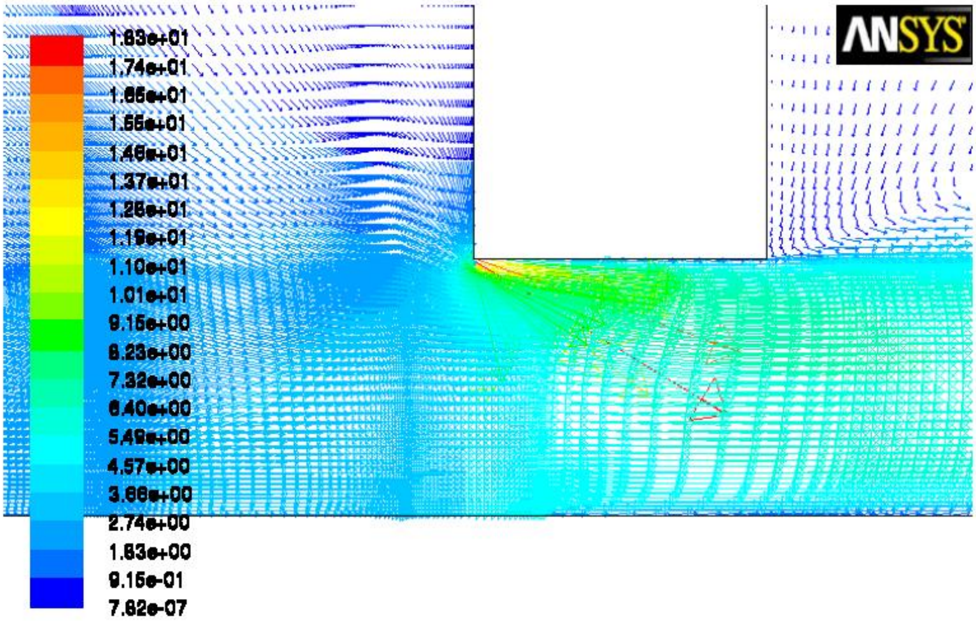

Fig. 5.22 Velocity vector field for compressible flow

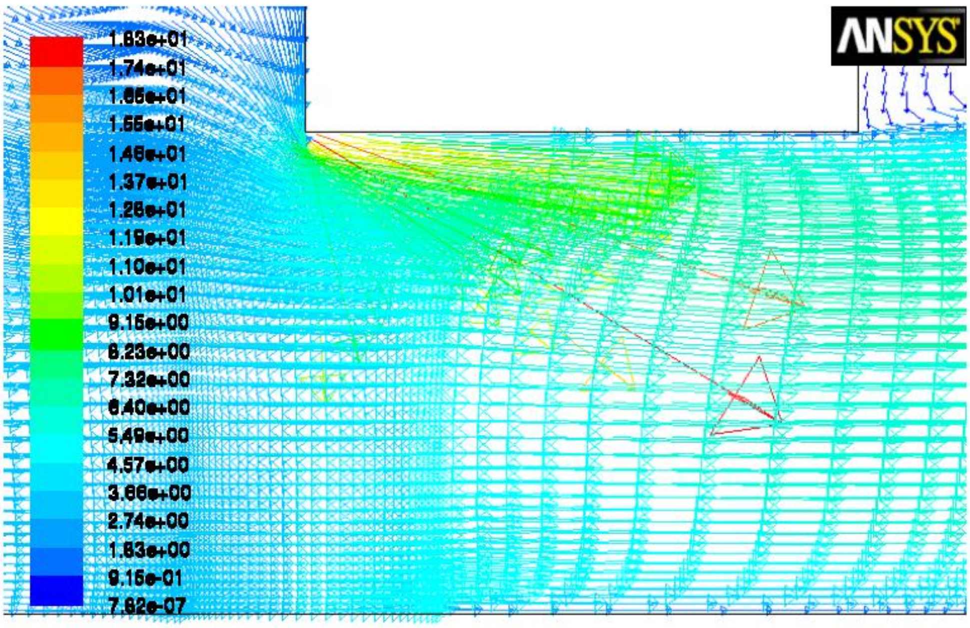

Fig. 5.23 Velocity vector field more detailed for compressible flow

5.7 Results Part 3 – Clearance Effect

Brush seal technology gives a very important advantage for the engine performance than the other types of sealing, especially than labyrinth seals. But there are also still some obstacles such as bristle wear, increase of leakage flow to overcome to labyrinth seals.

It can be seen a performance loss at the brush seal applications,

- due to the leakage of high pressure air passing the combustion chamber and turbine rotor blades,
- with the spoiling effect as the leakage flow returns to main turbine,
- increasing of p_d due to the additional Leakage flow, which affects the fine balance of the bearing loads.

On the other hand the possible smallest flow is not always the most important thing in design. Sometimes a predictable and stable leakage is important and desired. Thus it is easier to keep the bearing loads within their design specifications and to maintain optimum turbine efficiency. It can be possible by designing a brush seal with an initial "running" clearance.

Ferguson showed that by having an initial running clearance, the leakage flow would still be a quarter to one fifth of what would be expected through an annular gap with similar dimensions. But some studies [11] show this to be slightly optimistic. The difference was put down to an effect, where the bristles close down the clearance under the influence of the differential pressure across the brush seal. This effect is called "Blow Down" which is known to be due to the radial inward flow within the brush pack.

In other words, the bristles are pushed toward the rotor and reduce the clearance formed by the tip wear. Blow down effect can cause to the bristle wear problem also. But for bristle wear, there are also another reasons too, like brush instability, flutter due to aerodynamic excitation, rotor run out, eccentricity etc.

Finally it can be said that some applications require the brush seal which is designed with some initial clearance. On the other hand, a steady state clearance is needed for cooling purposes and purge flow [15]. Some special applications may also require seal clearance only during start up or shut down.

After giving the information about the clearance effect, here it is explained how it is modeled and simulated in present work. It is used the same geometry from Bayley and Long [1] ,Chew et al. [11]and it is given four different clearances:

$$z_1 = 0{,}27mm$$

$$z_2 = 0{,}75mm$$

$$z_3 = labyrinth(1.4mm)$$

$$z_4 = full\,brush(without\ gap)$$

In **Fig 5.24** to **5.27**, it is showed the geometries with mesh.

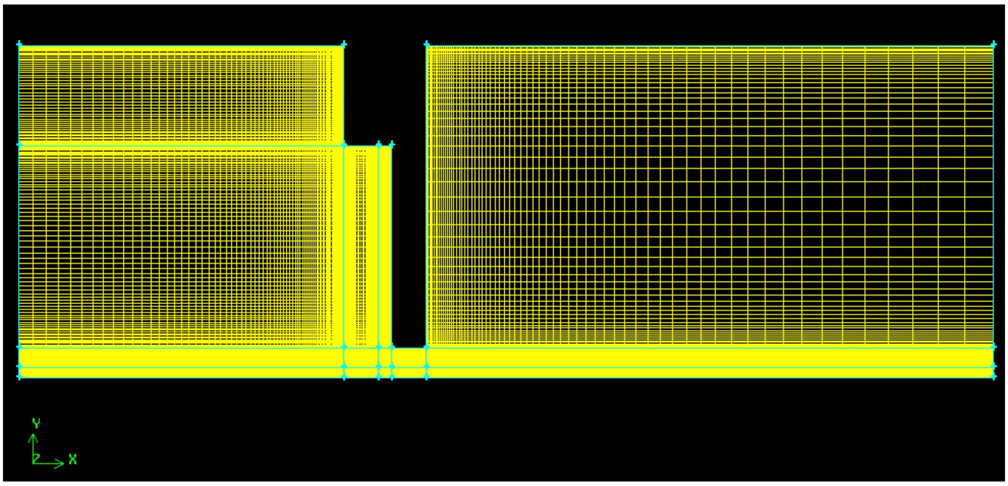

Fig. 5.24 Clearance for 0,27mm the whole figure

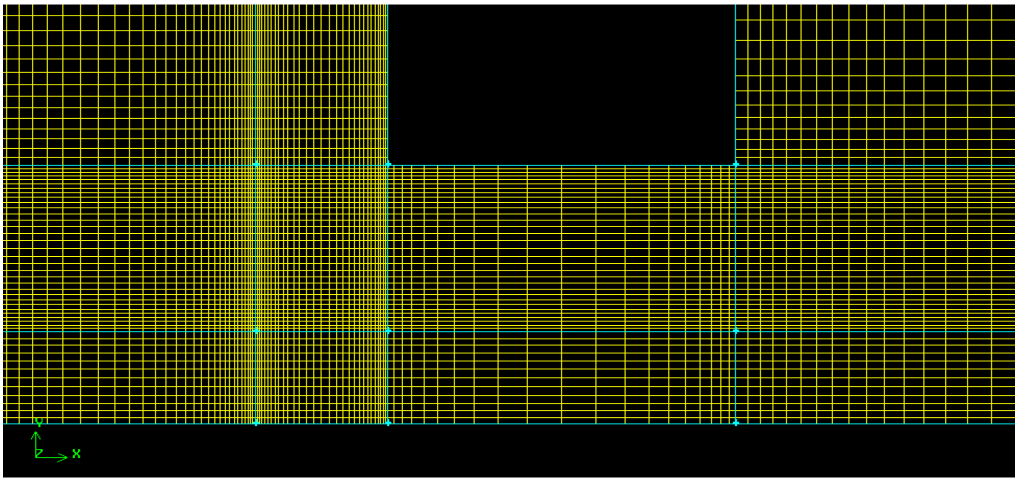

Fig. 5.25 Clearance for 0,27mm brush seal area

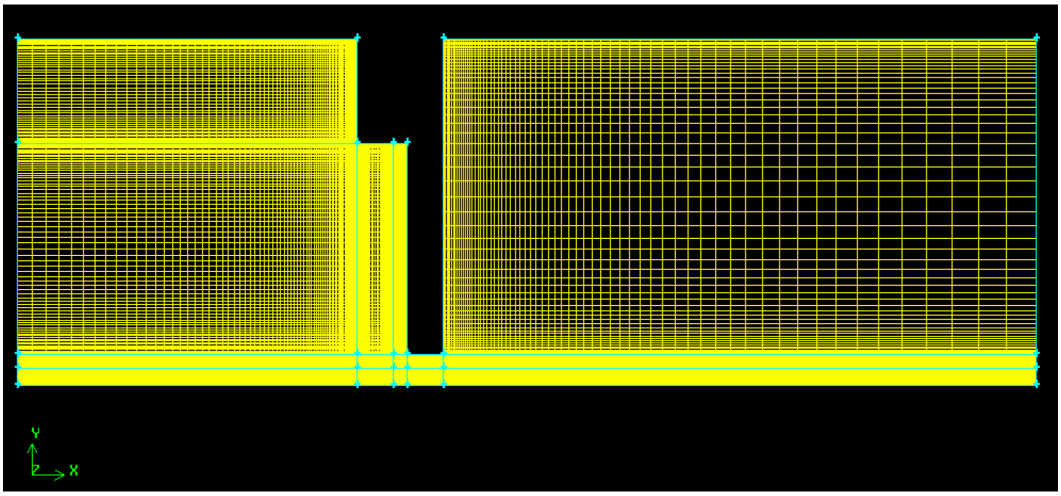

Fig. 5.26 Clearance for 0,75mm whole figure

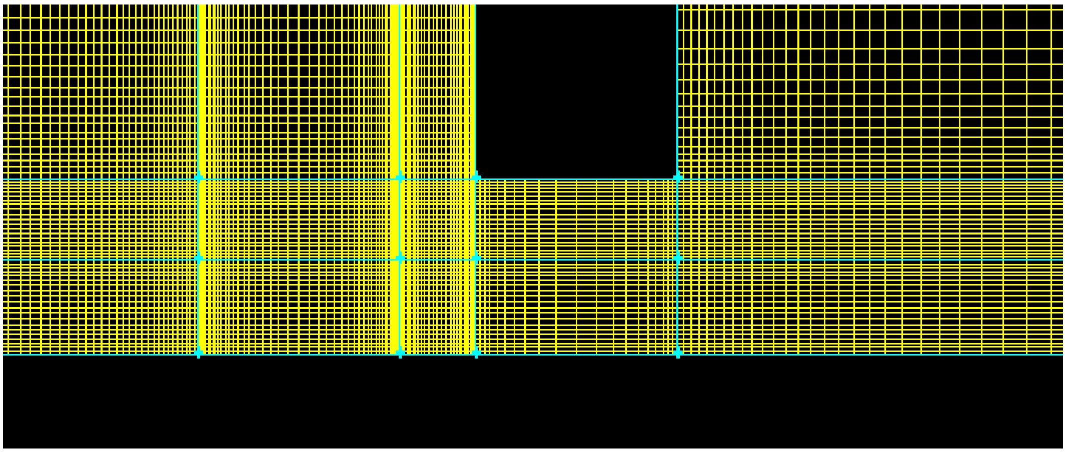

Fig. 5.27 Clearance for 0,75mm bristle pack area

These geometries for clearance are selected from Chew et al [11]. These are the clearance measurements that they are used in researches often.

As it is mentioned before in **Part 1**, it is seen that, it is used denser mesh at the brush region and clearance area. Because the pressure drop occurs along the brush, at the same time the flow try to pass through the clearance. Therefore for the better solutions, mesh should be generated with good density.

The leakage flow is that is driven by the pressure difference across the brush seal is assumed turbulent and compressible.

The $k - \epsilon$ model is used for the turbulent flow. The ideal gas law is applied for the compressible air flow. Constant air properties are evaluated at cavity temperature and atmospheric pressure conditions. Pressure boundary conditions are imposed at the inlet and exit boundaries.

Further information about simulation is:

- Downstream boundary is kept at atmospheric pressure,
- The pressure ratio Rp is varied from 1.1 to 4,
- The air inlet temperature is set constant at 20 ^{o}C,
- The rotor is considered as stationary in the present investigation.

For the solution methods coupling method is used and it has to apply serial analyses. It means the analyses begin with $\boldsymbol{R_p} = 1{,}5$ and than after one point, for ex 2500 iteration, $\boldsymbol{R_p}$ increases to 2. This means the iterations increase step by step.

At the next topic, the results will be discussed.

In this work, the compared data is taken from the experimental work which is carried out Chew et al. [11] who these results further calibrated for the CFD Models.

5.7.1 Mass Flow Rate

In **Figure 5.28** and **5.29**, the variation of measured mass flow through the brush seal with pressure ratio versus radial build clearance is shown.

On the graph, there are three different data to compare. These are the experimental data from Chew et al [11], and the CFD data from the simulations, which is for compressible and also for incompressible flow applied. As the boundary conditions for compressible flow, pressure-inlet and pressure-outlet and for incompressible flow, mass flow inlet boundary conditions are applied.

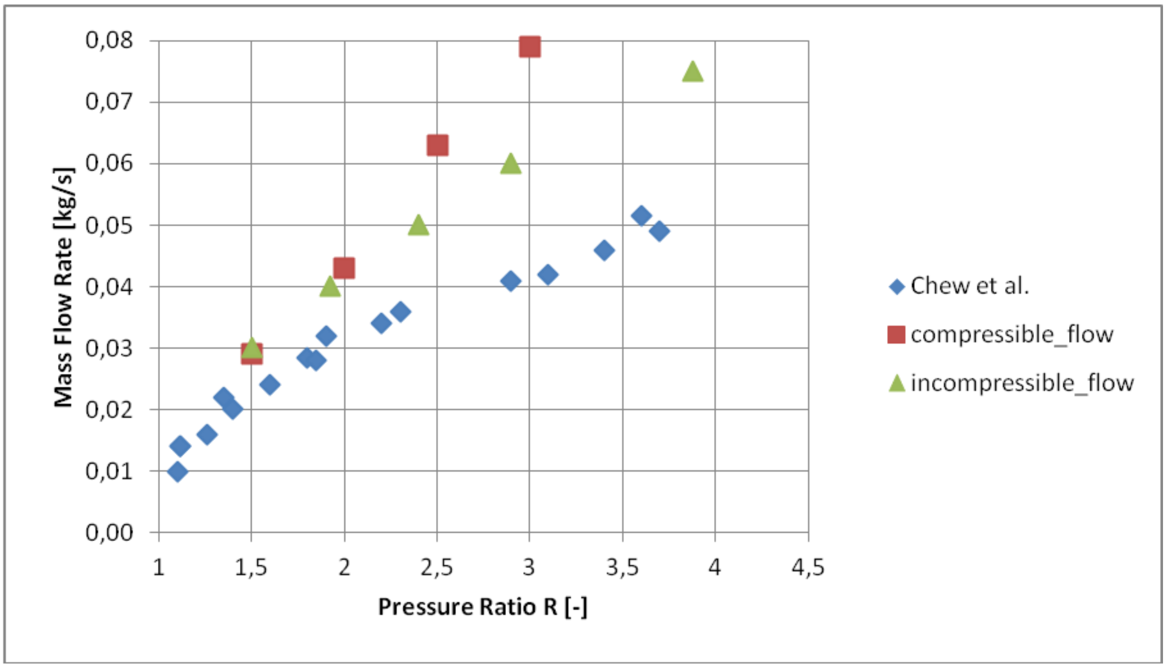

Fig. 5.28 Mass flow rates for cl=0,27mm

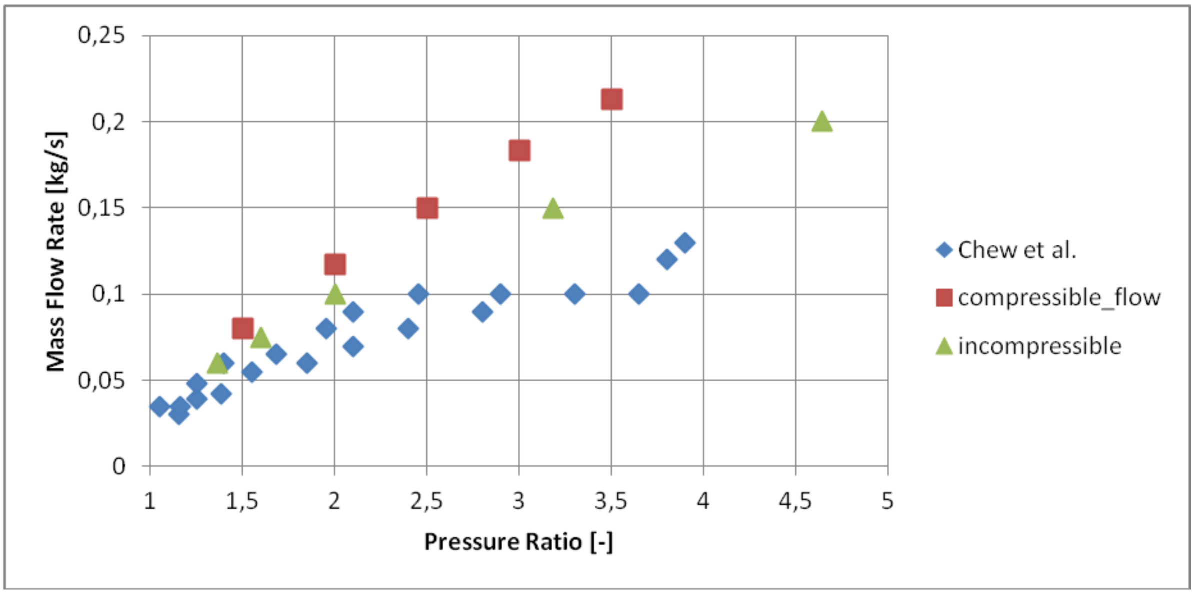

Fig. 5.29 Mass flow rates for cl=0,75mm

As is to be expected, the mass flow is strongly dependent on the radial build clearance. The mass flow through the seals increases for any clearance with pressure ratio. **Figure 5.30** shows four different leakage behaviors from the simulations.

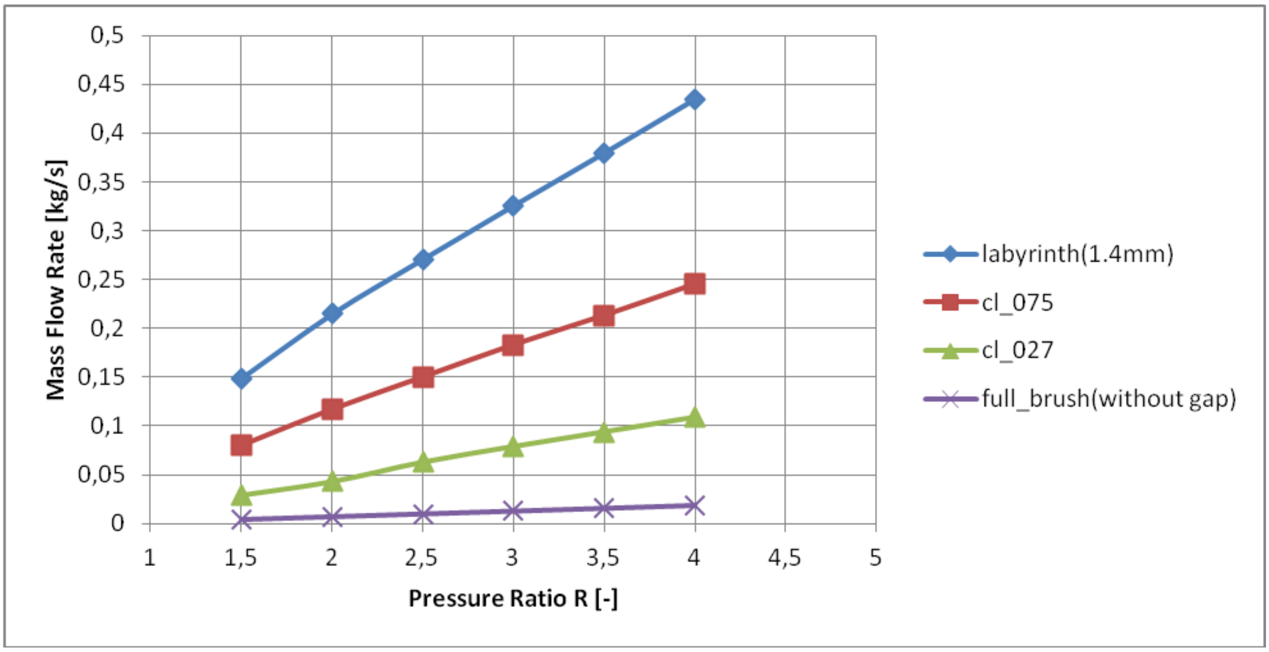

Fig. 5.30 Mass flow rate vs. pressure ratio for four different brush type

If the results are generally examined, it can be seen a overestimating from the experimental data. It can be explained with, whether the analyses applied with blow-down or not blow down effect. The CFD simulations were applied without blow-down effect. It can be arranged by the porosity of the brush seal in the simulation. This topic is investigated by Dogu and Aksit [14]. They observed that (it is also observed by Chew et al. [11]) when no blow-down effect by the simulations is considered, the CFD results overestimates the experimental data for high-pressure ratio cases. It can be see also from the **Fig. 5.28** and **Fig.5.29** clearly. This indicates existence of partial blow-down at high pressure ratio cases where clearance gradually reduces. A slight decrease in clearance results is a considerable drop in leakage. To capture this effect, a gradually blow-down can be modeled to match exact experimental leakage rates [14]. In this work, the simulations are executed without blow-down effect.

5.7.2 Axial Pressure Distribution

The calculated axial-pressure distribution on the rotor surface is shown in the **Fig. 5.31** and **Fig. 5.32**. As seen from these two figures, the pressure drop starts in front of the bristle pack due to flow acceleration through the clearance or in other words, at the upstream face of bristle pack. For both situations, for compressible and incompressible flow, most of the pressure drop occurs at the downstream side of the bristle pack. It can be explained with the compressibility and flow expansion effects.

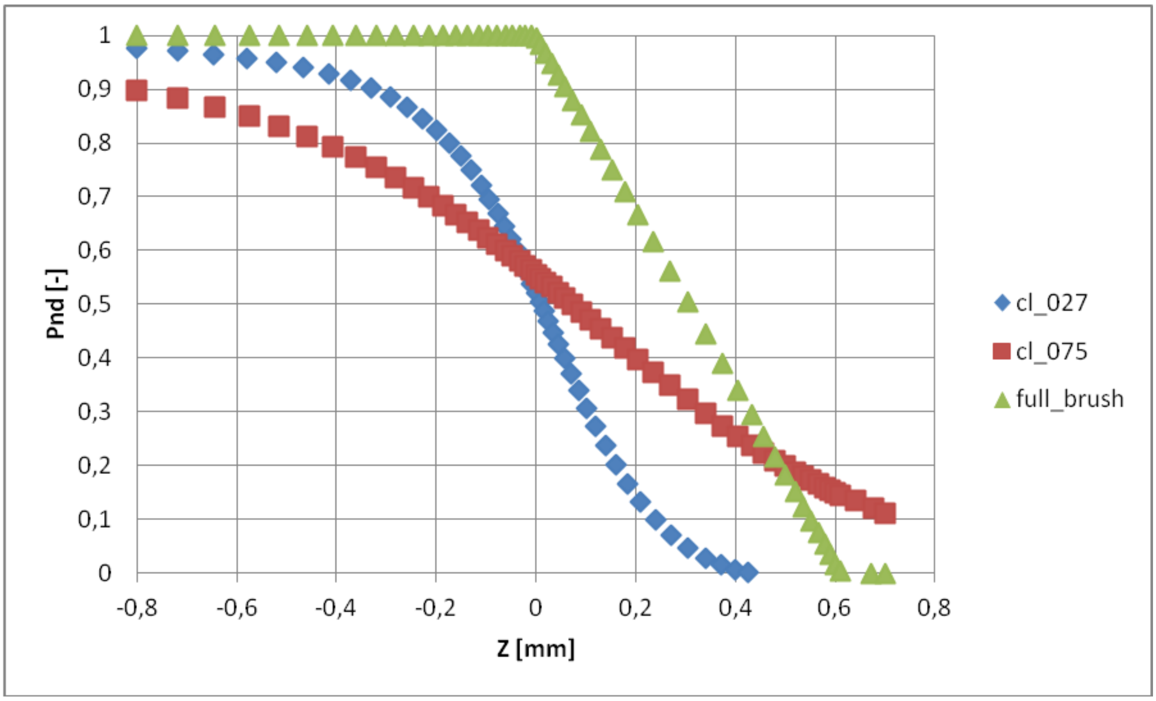

Fig. 5.31 Axial pressure distribution for incompressible flow

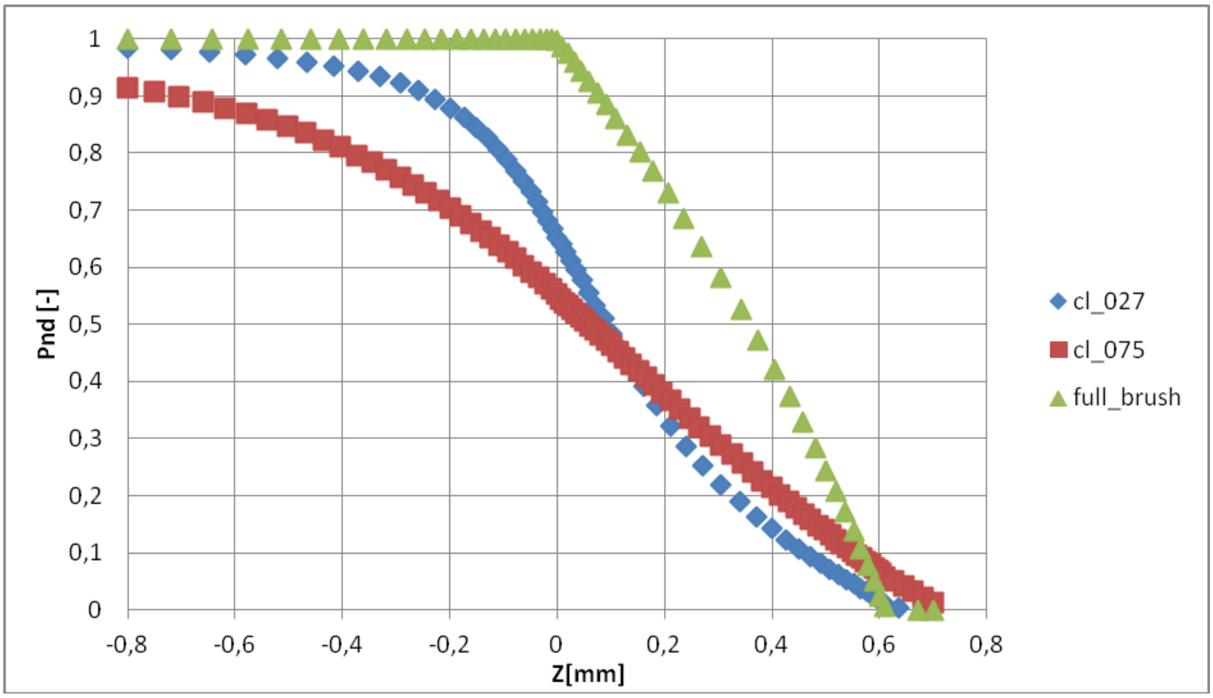

Fig. 5.32 Axial pressure distribution for compressible flow

As it is mentioned in the researches [1,11], the axial pressure distribution on the rotor surface doesn't follow a linear drop for the brush seal. And it is known that the results are in agreement with some of the earlier works (see in the previous section). But for the clearance seal, the axial pressure drop shows after one point approximately a linear trend compared to the contact seal.

The difference between two flow types can be seen in **Fig. 5.31** and **5.32**. The axial pressure distribution is nearly same for both simulations. For the compressible flow analyses, the pressure gradient follows more linear than the incompressible flow.

The simulations with 0,27mm and 0,75mm clearance for the compressible flow pressure gradient shows also similar behavior.

5.7.3 Radial Pressure Distribution

In **Fig. 5.33** and **Fig. 5.34** is shown the distribution of the non-dimensional pressure p_{nd} versus the non-dimensional distance ***Y***. ***Y*** is the coordinate in radial direction at the interface between brush and backing plate. The origin is located at the rotor surface and ***Y=1*** indicates the corner between the bristle pack and the front plate. Non-dimensionality is explained in the previous section.

Most of the radial pressure drop occurs in the half of the free bristle height near the rotor surface. The pressure at the upper side is nearly same with the upstream pressure. The pressure drop occurs in the region of down backing plate and downstream pressure is gained at this area.

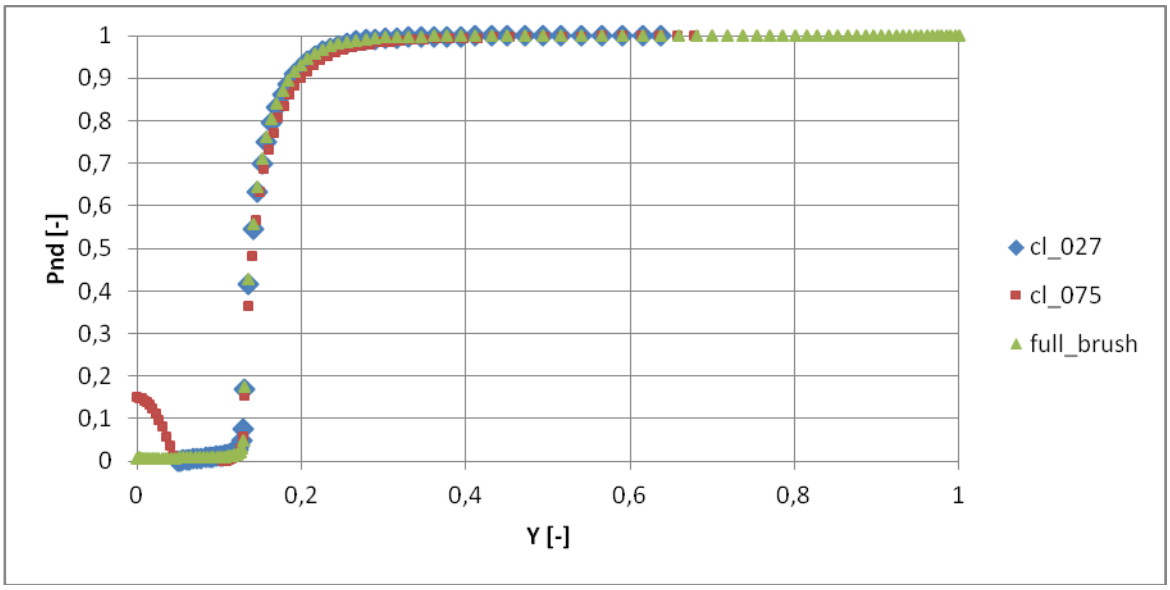

Fig. 5.33 Radial pressure distribution for incompressible flow

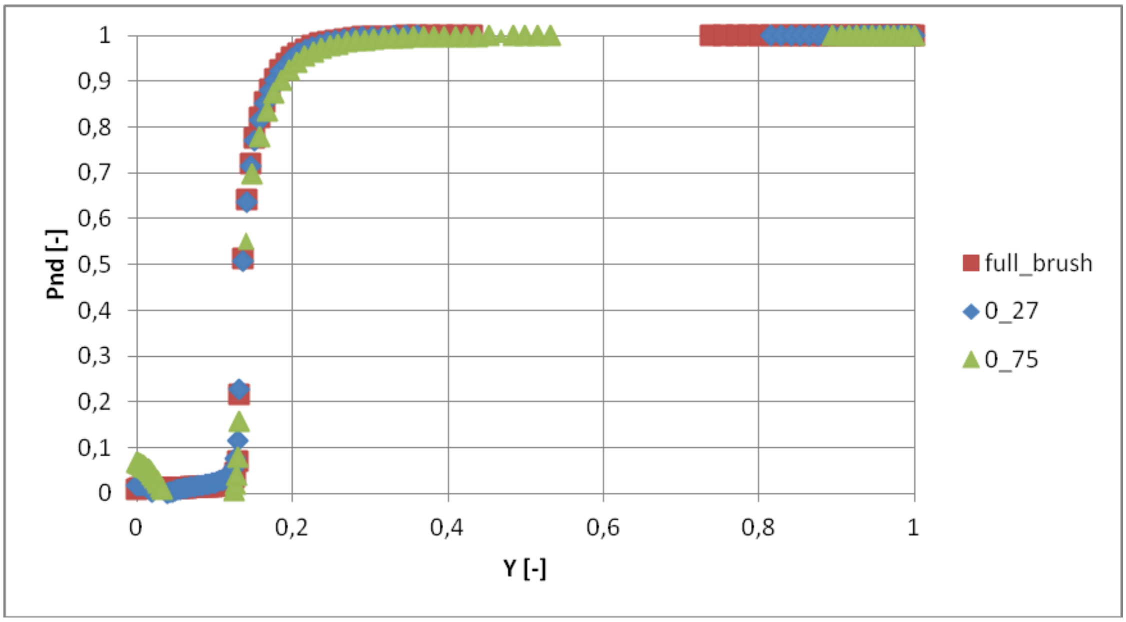

Fig. 5.34 Radial pressure distribution for compressible flow

The radial flow accelerates toward the rotor as axial diffusions add more mass flow. This confirms the observed radial pressure gradient. The radial pressure gradient governs the inward radial flow which is driving to the blow-down effect [14].

5.7.4 Flow Fields and Flow Behavior

In **Figure 5.35** to **5.42**, it is shown the comparison of clearance seals by using contour plots for pressure, axial velocity and radial velocity. It is known that, the most of the pressure drop occurs at the downstream side of the bristle pack for the full-brush (contact) seals.

For the brush seal simulations with clearance it is a little different. Because of the clearance gap, the pressure drop is distributed over the thickness of the bristle pack.

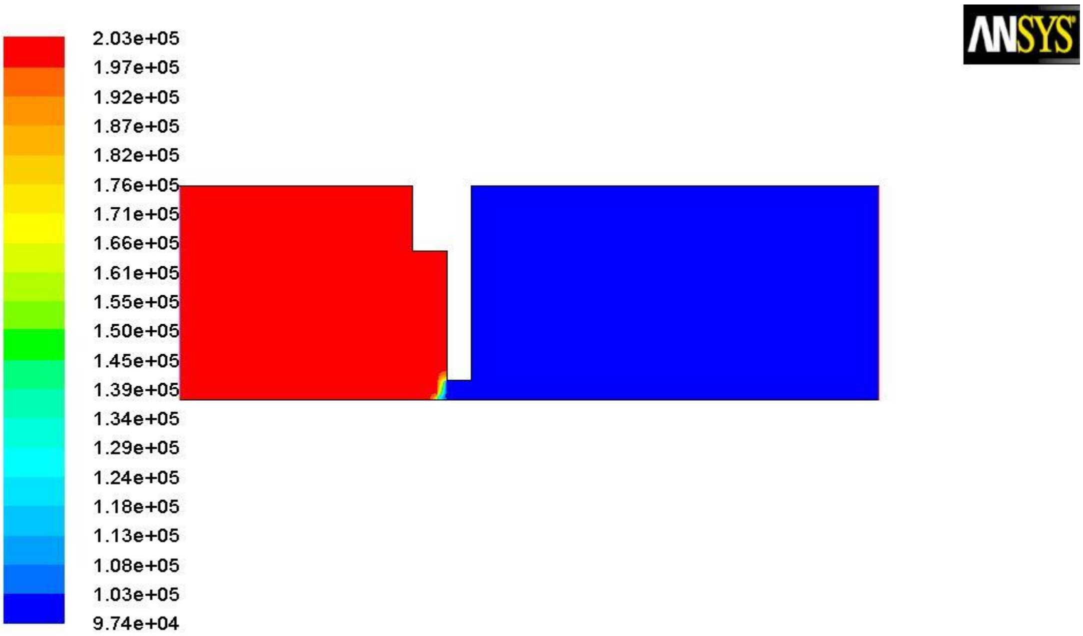

Fig. 5.35 Contours of absolute pressure for compressible flow with 0,27mm clearance

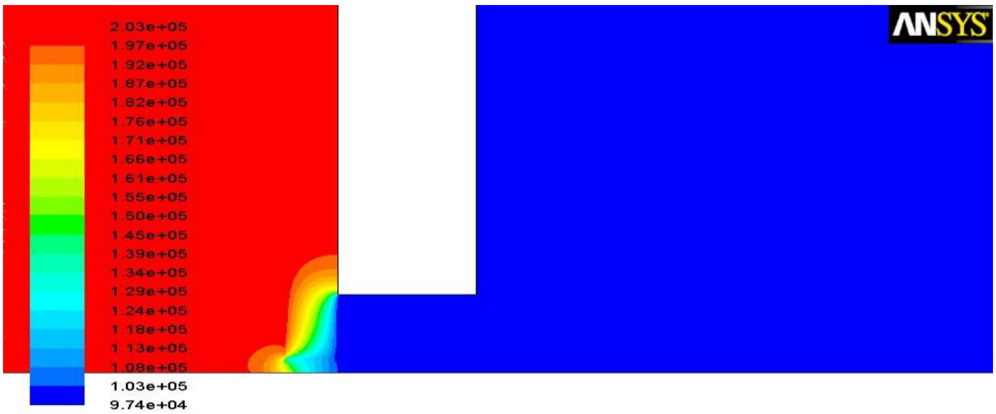

Fig. 5.36 Contours of absolute pressure for compressible flow with 0,27mm clearance with more detail

For the velocities, radial velocity contours show different distribution for each simulations. At the clearance area, the flow accelerate with the entrance of clearance and because of this, a strong radial flow develops. In **Figure 5.38** it can be seen.(**Figure 5.41** shows more details)

The same situation can be seen for the axial velocities in **Fig. 5.37**. The axial flow is also accelerated at the clearance entrance due to flow acceleration.

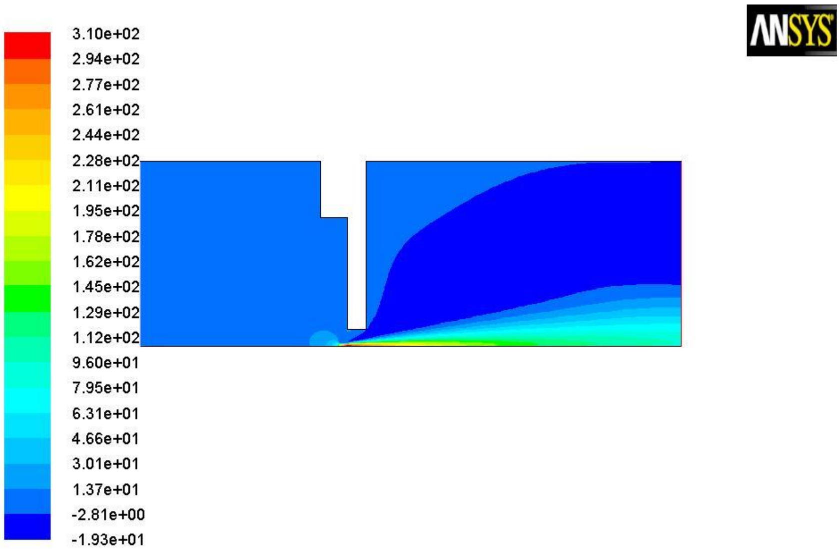

Fig. 5.37 Contours of axial velocity for compressible flow with 0,27mm clearance

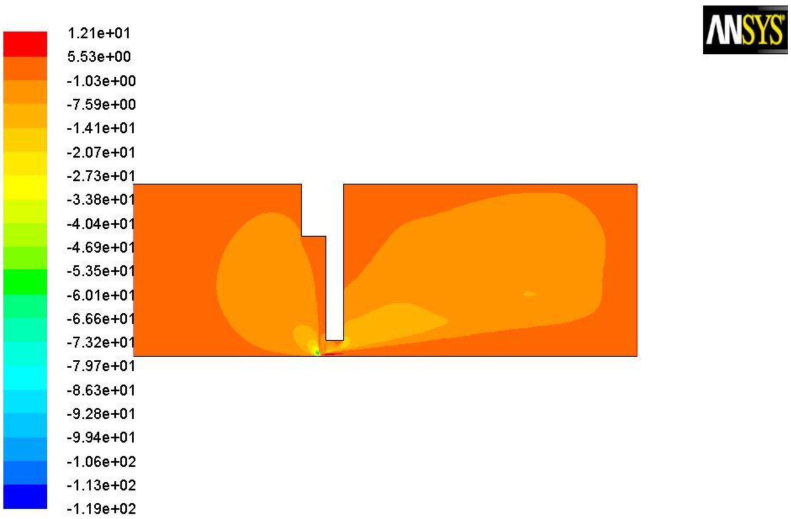

Fig. 5.38 Contours of radial velocity for compressible flow with 0,27mm clearance

Figure 5.39 to **5.42** show more detailed velocity flow distribution for 0,27mm and 0,75mm clearance. For the axial velocity, with entering to the clearance area, the velocity magnitudes reach quickly to high values and it is seen clearly in the **Fig. 5.39** and **5.40**. For the radial velocity, at the corner of the down side of the brush there is a changing but after this point it takes normal form again and it can be also clearly seen in **Fig. 5.41**and **5.42**.

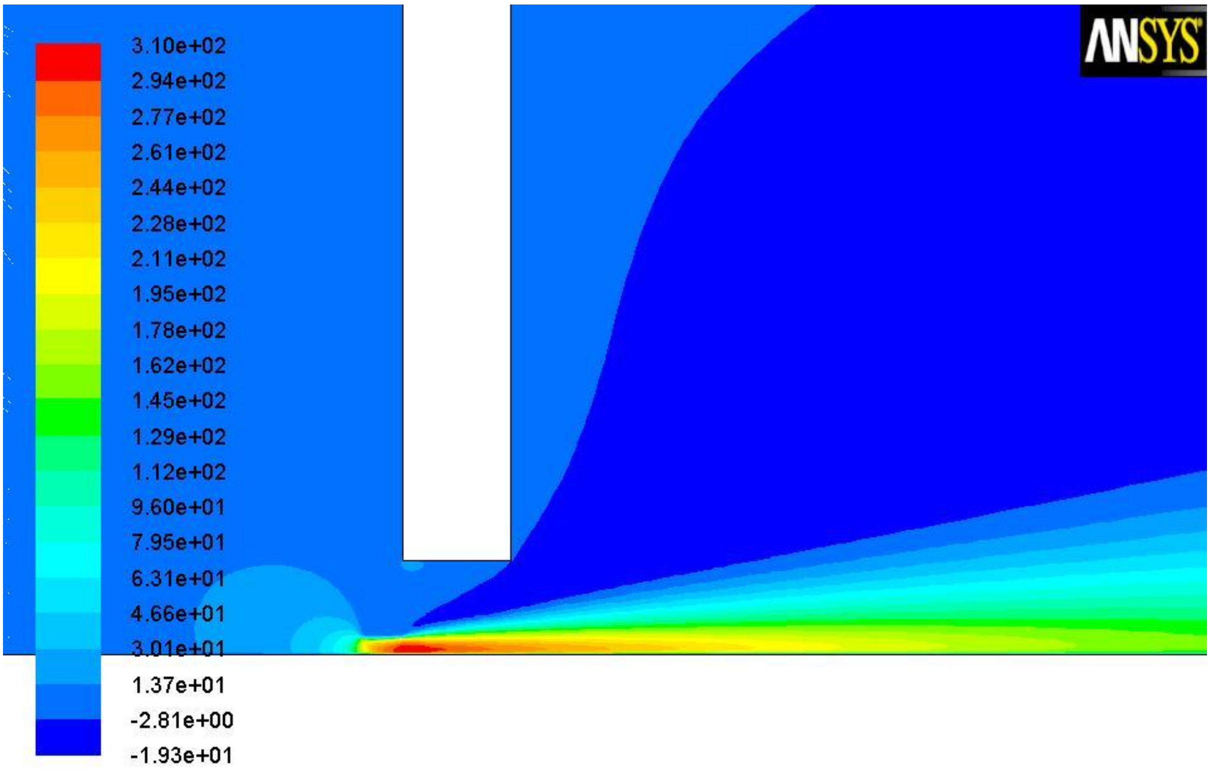

Fig. 5.39 Contours of axial velocity for compressible flow with 0,27mm clearance

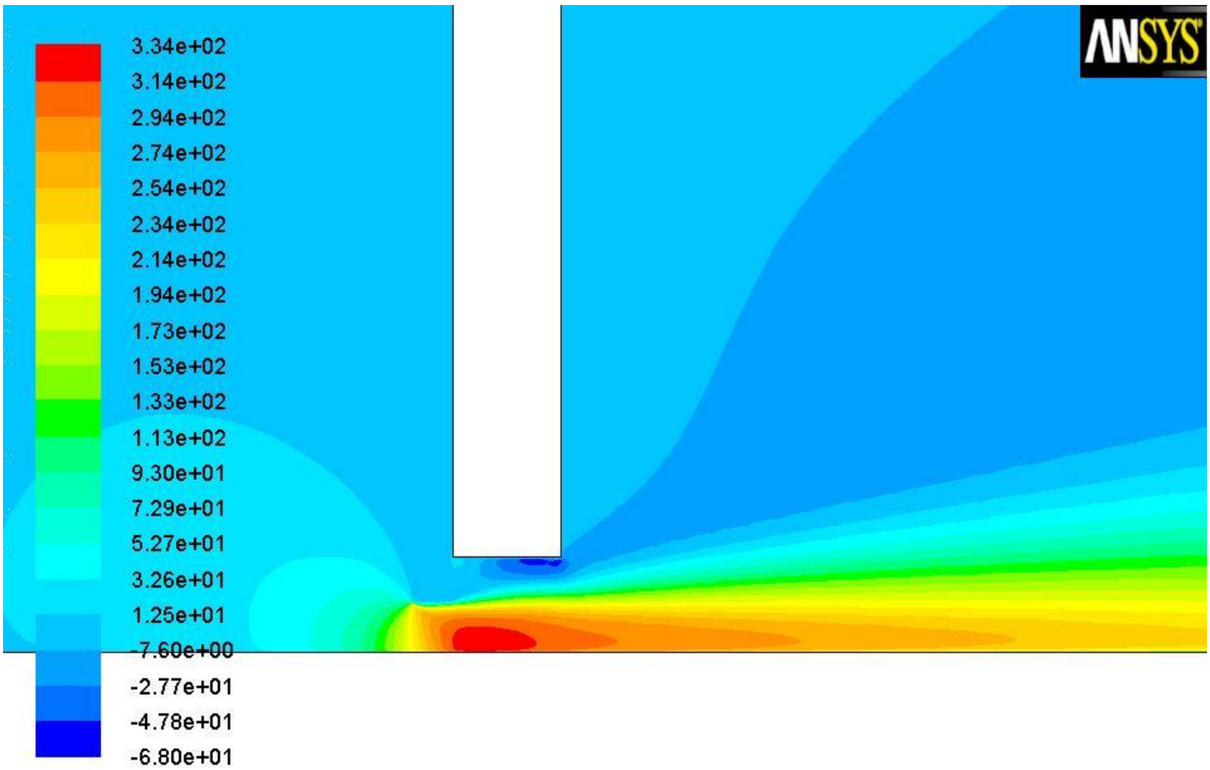

Fig. 5.40 Contours of axial velocity for compressible flow with 0,75mm clearance

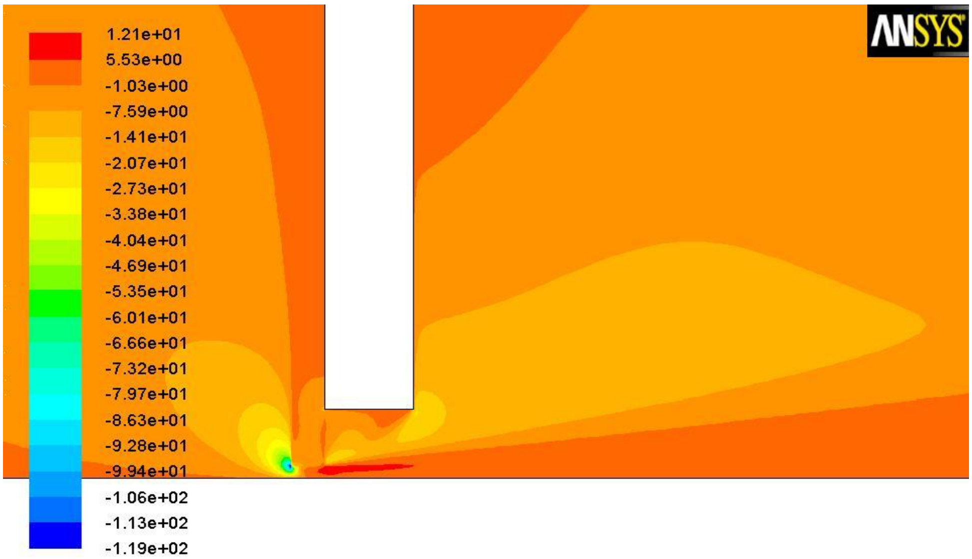

Fig. 5.41 Contours of radial velocity for compressible flow with 0,27mm clearance

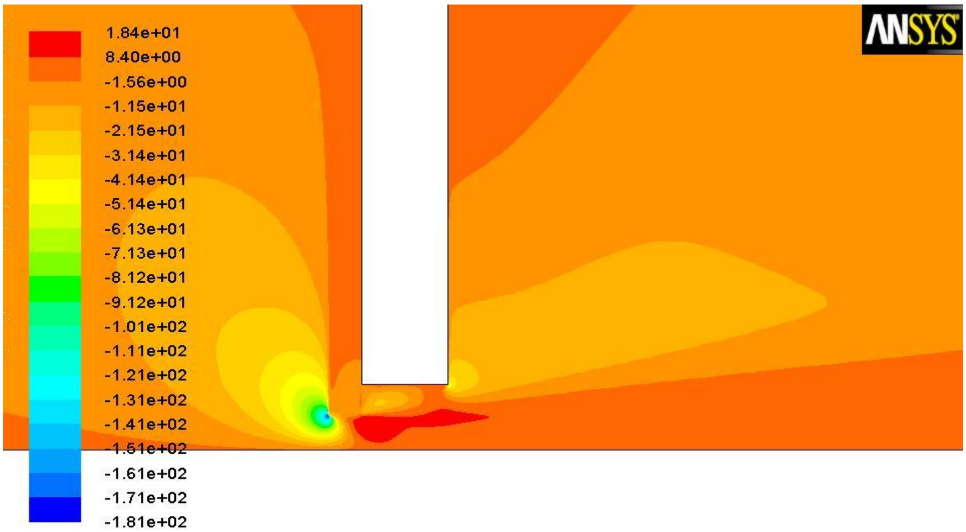

Fig. 5.42 Contours of radial velocity for compressible flow with 0,75mm clearance

The fence height region is always critical for the brush seal flow and dynamic behavior of the brush. Normally, without clearance the flow comes till brush axial and with the brush it is formed to the radial flow. It can be seen from the vector distribution in **Fig 5.43** and **5.44**. It goes through the bristle pack with radial and this radial flow turns axial again and discharges to downstream of the fence height region under the backing plate.

At the clearance area, the axial flow through the gap under the brush is strong. Therefore the velocity magnitude reaches high values in front of the bristle pack at the upstream of the clearance region. The flow through the clearance expands to the downstream cavity from higher to lower pressures. In **Figure 5.43** and **5.44**, it is clear to see the movement of the flow with vectors.

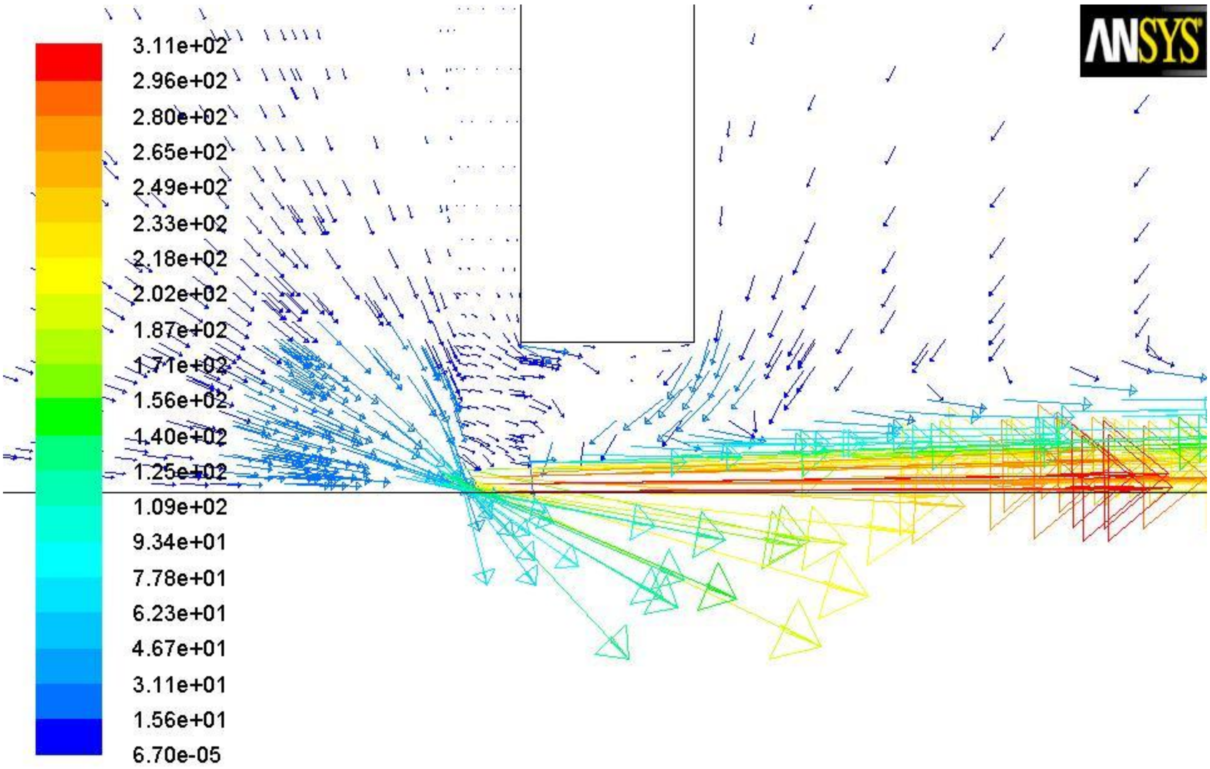

Fig. 5.43 Vector flow for 0,27mm clearance brush seal

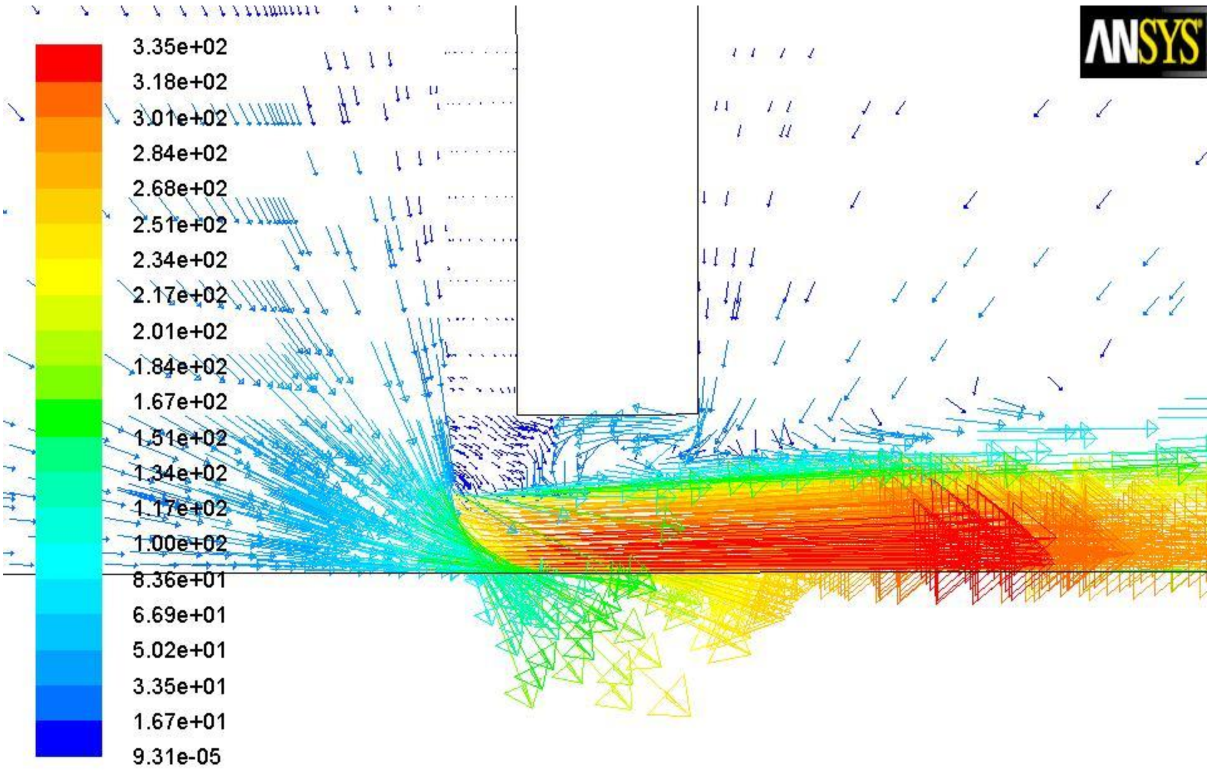

Fig. 5.44 Vector flow for 0,75 mm clearance brush seal

6. Summary and Conclusion

In present work, the simulations are applied with ANSYS-FLUENT and results are compared with experimental values which is found by Bayley and Long [1] and Chew et al.[11] Two different type of model are investigated. These are brush seal applications with and without radial clearance. Experimental data [1, 11] are used as reference point. With present work, it is tried to come close to these reference values and to create an accurate CFD model of brush seal. Nevertheless the usability of commercial CFD Software is checked. With ANSYS, GAMBIT is used to generate the geometry of model. In GAMBIT, mesh structure is given. Mesh on model has an important role to simulate problem accurately. ANSYS gives more accurate results with good mesh. Especially in flow analyses, mesh quality is important for flow to be formed. Otherwise, if the flow isn't formed, it is impossible to become exact solutions. Reaching a complete accurate mesh structure is not always possible, therefore in present simulation, it is tried to come close optimum mesh.

Modeling of brush is difficult. In procedure of simulating the brush seals using a porous medium in order to gain information about flow characteristics has become accepted and used. It is also used in present work.

If the results are examined, there are some deviations between CFD results and experimental data. This can be related to the modeling of problems with GAMBIT and simulating with ANSYS. In CFD simulations, it is tried to get experimental values which are found under the real conditions. But in CFD, values are entered which is generated with mathematical relations from experimental results. It is very complicated to catch real situations in CFD. But with the development of CFD technique, day by day the results are come close to experimental results. Therefore for the present work, the deviations are not critic and they are acceptable. Two different brush seal model is compared with experimental data. Brush seals without clearance give better simulation results than brush seal with clearance. As it is before mentioned, the model with radial clearance has problem with simulating brush. It is here difficult to find out whether it is modeled with the consideration of blow-down effect or not. It is very complicated theme. Dogu [14] has done many investigations about it. In present work, no blow down effect is taken. Even so, the results are similar with the experimental values.

Finally, sealing is very important in turbo machinery and sealing technology is in development and improvement. Using of CFD technique with this development is increased too. Because using of CFD is more practical and cheap. Finding the optimum sealing type is another theme. Labyrinth seals are expired slowly. On the other hand, brush seals give still good results. As it seen from this work, brush seals with radial clearance give better solutions than labyrinth seals but still worse than brush seals without radial clearance. The point is here blow-down effect on brush. It can be more investigated.

There are many researches on the sealing applications. As it seen in **Chapter 2**, designers try to find best sealing applications with low price. Nevertheless, day by day, using of CFD is taking more part on the investigations.

BIBLIOGRAPHY

[1] **Bayley F. J., Long C. A.:** A Combined Experimental and Theoretical Study of Flow and Pressure Distributions in a Brush Seal. Journal of Engineering for Gas Turbines and Power. Vol. 115 (April 1993)

[2] **Willinger R. :** Computation of the Flow in Turbomachinery Brush Seals Using a Porous Medium Approach. (2005)

[3] **Stanisław Michał Cieślewicz:** 2004. CFD-Simulations for Advanced Turbomachinery Sealing Technologies: Brush Seals

[4] **Sabri Ergun:** 1952. Chemical Engineering Progress, Vol.48, No. 2

[5] **Pröstler S.:** CFD Modeling of Brush Seals. European CFX Conference (September 2002)

[6] **Robert C. Hendricks, Raymond E. Chupp, Scott B. Lattime, Bruce M. Steinetz:** Turbomachine Interface Sealing, NASA/TM—2005-213633

[7] **Raymond E. Chupp, Robert C. Hendricks, Scott B. Lattime, Bruce M. Steinetz:** Sealing in Turbomachine, NASA/TM—2006-214341

[8] **Chew J.W., Lapworth B.L., Millener P.J.:** Mathematical Modeling of Brush Seals. International Journal of Heat and Fluid Flow. Vol. 16, No. 6(1995)

[9] **Chupp, R. E., Aksit, M. F., Ghasripoor, F., Turnquist, N. A., and Demiroglu:** M., 2001, "Advanced Seals for Industrial Turbine Applications," AIAA Paper No. 2001-3626.

[10] **Chen L. H., Wood P. E., Jones T. V., Chew J. W.:** Detailed Experimental Studies of Flow in Large Scale Brush Seal Model and a Comparison with CFD Predictions. Journal of Engineering for Gas Turbines and Power. Vol.122 (October 2000)

[11] **Turner M.T., Chew J.W., Long C.A.:** Experimental Investigation and Mathematical Modeling of Clearance Brush Seals. ASME Paper No. 97-GT- 282 (September 1997)

[12] **Gernot Bischelmaier:** Simulation des Strömungsverhaltens in einer Lamellendichtung mittels porösem Medium. Diploma Thesis, TU Vienna, 2011

[13] **Jun LI*, Yangzi HUANG, Zhigang LI, Zhenping FENG:** ASME Paper GT2010-22877.

[14] **Yahya Dogu, Mahmut F. Aksit, Mehmet Demiroglu, Osman Saim Dinc:** Evaluation of Flow Behavior for Clearance Brush Seals. Journal of Engineering for Gas Turbines and Power JANUARY 2008, Vol. 130 / 012507-9

[15] **Dinc S., Demiroglu M., Turnquist N., Mortzheim J., Goetze G., Maupin J., Hopkins J., Wolfe C., Florin M.:** Fundamental Design Issues of Brush Seals for Industrial Applications. Journal of Turbomachinery (April 2002)

[16] **O'Neill, A. T., Hogg, S. I., Withers, P. A., Turner, M. T., and Jones:** T. V., 1997, "Multiple Brush Seals in Series," ASME Paper No. 97-GT-194.

[17] **Aksit, M. F.:** A Computational Study of Brush Seal Contact Loads with Friction. Ph.D. thesis, Rensselaer Polytechnic Institute, Troy, NY.

[18] **Crudgington, P. F., and Bowsher, A.:** Brush Seal Blow Down. AIAA Paper No. 2003-4697.

[19] **Chew J.W., Hogg S.I.:** Porosity Modeling of Brush Seals. Journal of Tribology (1997)

[20] **Chupp R. E., Nelson P.:** Evaluation of Brush Seals for Limited-Life Engines. Journal of Propulsion and Power. Vol. 9 (January 1993)

[21] **Dogu Y.:** Investigation of Brush Seal Flow Characteristics Using Bulk Porous Medium Approach. ASME Paper No. GT2003-38970 (June 2003)

[22] **Braun M. J., Kudriavtsev V. V.:** A Numerical Simulation of a Brush Seal Section and Some Experimental Results. Journal of Turbomachinery. Vol. 117 (January 1995)

[23] **Guardino C.:** Numerical Simulation of 3D Bristle Bending in Brush Seals. University of Surrey Research Report, FR/2002.13 (2003)

[24] **Guardino C., Chew J.W.:** Numerical Simulation of 3D Bristle Bending in Brush Seals. ASME Paper No.: GT2004-53176 (June 2004)

[25] **Chupp, R. E., Holle, G. F., and Dowler :** Simple Leakage Flow Model for Brush Seals. (C.A., 1991) AIAA paper no. 91-1913

[26] **Short J.:** Advanced Brush Seal Development. Higher Pressure Capabilities Using a Single Stage Brush Seal. AIAA 96-2907 (1996)

[27] **Patent:** General Electric Co, Ohio, USA, 2001, Patent number: US 6220815.

[28] **Salim .M. Salim, and S.C. Cheah :** Wall y+ Strategy for Dealing with Wall-bounded Turbulent Flows. Proceedings of the International Multi Conference of Engineers and Computer Scientists 2009 Vol. II IMECS 2009, March 18 - 20, 2009, Hong Kong

[29] GAMBIT Help Files

[30] FLUENT Help Files

[31] **Web address:** http://www.incarbons.com

[32] **Web address:** http://www.mcnallyinstitute.com

[33] **Web address:** http://www.omtr.pub.ro

[34] **Web address:** http://www.mtu.de